Human motor unit discharge patterns reveal differences in neuromodulatory and inhibitory drive to motoneurons across contraction levels

Jakob Škarabot[1*], James A Beauchamp[2,3], Gregory EP Pearcey[3,4,5*]

[1]School of Sport, Exercise and Health Sciences, Loughborough University, Loughborough, UK

[2]Department of Biomedical Engineering, McCormick School of Engineering, Northwestern University, Chicago, IL, USA

[3]Department of Physical Therapy and Human Movement Sciences, Feinberg School of Medicine, Northwestern University, Chicago, IL, USA

[4]School of Human Kinetics and Recreation, Memorial University of Newfoundland, St. John's, Canada

[5]Division of BioMedical Sciences, Faculty of Medicine, Memorial University of Newfoundland, St. John's, Canada

*Correspondence: J.Skarabot@lboro.ac.uk ; gpearcey@mun.ca

ABSTRACT

Transformation of motor commands via a motor unit (MU) into mechanical actions of muscle fibres is a non-linear function influenced by ionotropic excitatory/inhibitory and neuromodulatory inputs. Neuromodulatory inputs facilitate dendritic persistent inward currents on motoneurons, which introduce non-linearities in MU discharge patterns allowing estimation of the structure of motor commands. We investigated the relative contribution of neuromodulation and the pattern of inhibition to human MU discharge patterns with increasing contraction force. In Experiment 1, we identified MU discharges in tibialis anterior, and vastus lateralis and medialis during isometric triangular dorsiflexion and knee extension contractions, respectively, up to 70% of maximal voluntary force (MVF). We quantified the onset-offset hysteresis (ΔF) and performed quasi-geometric analyses of MU discharge patterns to quantify the magnitude of non-linearity, and slopes of MU discharge patterns during the acceleration and rate attenuation regions. We show that ΔF increased, whereas discharge patterns became more linear and had lower slopes at greater contraction forces. Experiment 2 required participants to dorsiflex up to 70% MVF with either matched duration or rate of force increase to determine if these factors were confounding the modulation in MU discharge patterns across contraction forces. Though ΔF and the magnitude of non-linearity were influenced by contraction duration, the relative changes in these variables across contraction forces were similar to Experiment 1. The results suggest that neuromodulatory input and patterns of inhibition are uniquely shaped to support force increases across a large proportion of the motor pool's recruitment range in three human lower limb muscles.

Key words: High-density surface electromyography, decomposition, motor neuron, monoamines, persistent inward currents.

INTRODUCTION

All motor commands flow through alpha (i.e., spinal) motoneurons, which are the final common pathway for movement generation (Sherrington, 1925). An alpha motoneuron and all its innervated muscle fibres, collectively termed a motor unit (MU), transduce motor commands into muscle action potentials that generate mechanical actions (Heckman & Enoka, 2012). This transformation is a non-linear function influenced by both ionotropic and metabotropic inputs. Ionotropic inputs (e.g., corticospinal, reticulospinal, propriospinal, sensory, etc.) provide excitation (depolarisation) and inhibition (hyperpolarisation) to motoneurons, while metabotropic or neuromodulatory inputs modulate ionotropic inputs via G-protein coupled receptors. One potent source of neuromodulation is monoamines (i.e., serotonin (5-HT) and noradrenaline), which are released via long descending axons from the raphe nuclei and locus coeruleus that project diffusely throughout the spinal cord (Goaillard & Marder, 2021). Monoamines act on motoneurons to facilitate persistent inward currents (PICs) mediated by voltage-gated dendritic ion channels (Schwindt & Crill, 1980; Hounsgaard *et al.*, 1988; Bennett *et al.*, 1998; Binder *et al.*, 2020). These PICs provide an additional source of depolarisation that introduces non-linearities in motoneuron discharge by amplifying and prolonging excitatory ionotropic inputs (Lee & Heckman, 1998*a*, 2000). Whilst proportional to monoamines, PICs are also uniquely influenced by local inhibitory inputs, potentially allowing for insight into the structure of motor commands. More specifically, the action of PICs on motoneuron discharge is affected by tonic inhibitory inputs (Hyngstrom *et al.*, 2007) as well as the pattern of inhibition in relation to excitatory input (e.g., reciprocal vs. proportional patterns in relation to excitatory inputs; (Johnson *et al.*, 2012, 2017*a*). Tonic inhibitory input linearises MU discharge patterns (Revill & Fuglevand, 2017) and reduces estimates of PIC magnitude in humans (Mesquita *et al.*, 2022; Pearcey *et al.*, 2022), in agreement with prior studies in cat (Kuo *et al.*, 2003).

Whilst the importance of modulating excitatory ionotropic inputs for encoding muscle contraction force has received significant attention in both primates (Cheney & Fetz, 1980; Glover & Baker, 2022) and humans (Oya *et al.*, 2008; Weavil *et al.*, 2015), the degree to which changes in neuromodulatory inputs contribute to greater force production is less clear. Evidence in the cat has revealed that raphe neurons discharge at rates that increase with the increases in the speed of locomotion, which suggests that 5-HT release is tightly coupled with the intensity of motor output (Jacobs *et al.*, 2002). Pharmacological studies in humans further suggest that neuromodulatory drive mediated by 5-HT provides gain-control for voluntary force production (Wei *et al.*, 2014; Kavanagh *et al.*, 2019). However, whilst differences in the distribution of synaptic inputs to MUs of different thresholds likely mediate graded contraction force (Hultborn *et al.*, 2004), it is uncertain to what degree greater neuromodulatory inputs facilitate contractions at greater contraction forces.

Human studies of neuromodulatory inputs to motoneurons are highly inferential (i.e., see (Khurram *et al.*, 2022) for review) due to the unethical procedures required to directly record from spinal neurons. The most commonly employed method to estimate PICs and, thus, neuromodulatory drive to motoneurons in humans is the paired MU analysis technique that quantifies onset-offset hysteresis (delta frequency, ΔF; Afsharipour et al., 2020; Gorassini et al., 2002). However, when examined across different contraction levels, findings regarding ΔF remain inconclusive. ΔF has been shown to either increase (Orssatto *et al.*, 2021; Goodlich *et al.*, 2023) or remain

constant (Kim *et al.*, 2020; Afsharipour *et al.*, 2020) with increased voluntary drive. Although monoaminergic inputs likely vary between motor pools (Hounsgaard *et al.*, 1988; Wilson *et al.*, 2015) and could conceivably explain these varied findings, inconsistencies are still reported when examining the same muscle (Kim *et al.*, 2020; Orssatto *et al.*, 2021). Notably however, these studies have subtle methodological differences in their calculation of onset-offset hysteresis as well as their standardisation of the duration and rate of force increase, both of which have been suggested to influence ΔF (Vandenberk & Kalmar, 2014).

The potential modulation of inhibitory patterns has also been largely neglected in prior studies that have investigated the influence of contraction level on MU discharge rate profiles. Inhibitory patterns influence how motoneurons entrain the control of muscle fibres to produce force (Powers & Heckman, 2017), and thus contribute to the onset-offset hysteresis of pairs of MUs (Chardon *et al.*, 2022; Beauchamp *et al.*, 2023). Specifically, realistic simulations of motoneuron pools suggest that when the level of inhibition is reciprocal relative to the excitatory input, ΔF is likely to be greater compared to when inhibitory input increases proportionally to excitation (Chardon *et al.*, 2022).

Most importantly, prior studies examining motoneuron properties inferred from MU discharge patterns in humans have been largely restricted to relatively low contraction forces (<30% of maximum). This important detail both limits the investigation of discharge rate modulation to predominantly lower threshold MUs and restricts the range of behaviour to a level where intense neuromodulation may not be required to facilitate force outputs from the muscle. With increased voluntary contraction level, the already recruited MUs will increase their discharge rate, but the discharge rate modulation of these units in relation to their threshold remains uncertain. Classic motoneuron studies in reduced preparations suggested that the later-recruited, higher threshold motoneurons exhibit higher maximal discharge rates compared to lower-threshold neurons (Kernell *et al.*, 1983; Botterman *et al.*, 1986). However, whilst replicated in some experiments (Grimby & Hannerz, 1977; Moritz *et al.*, 2005; Oya *et al.*, 2009; Inglis & Gabriel, 2021), instantaneous discharge rates tend to be greater in lower- compared to higher-threshold human MUs when submaximal efforts are performed (Erim et al., 1996; Hassan et al., 2021; Person & Kudina, 1972), termed the onion skin phenomenon (for review see Pearcey & Rymer, 2022). The discharge behaviour of the same MUs across broad ranges of contraction levels, however, remains unexplored, largely due to the lack of appropriate methodologies to reliably decompose and track MUs with increased contraction level until recently (Francic & Holobar, 2021).

Here, we performed two experiments to characterise human MU discharge patterns across a wide range of contraction levels. The primary aim was to estimate the relative contribution of neuromodulation and the pattern of inhibition that contributes to MU discharge rate modulation with increasing force level. Estimates of PICs were quantified using an extensively validated and established computational approach of calculating onset-offset hysteresis of pairs of MUs (i.e., ΔF; Gorassini et al., 1998). However, this calculation is influenced by both monoaminergic neuromodulation and the pattern of inhibition (Chardon *et al.*, 2022; Beauchamp *et al.*, 2023). Thus, to gain further insight into the motor commands influencing MU discharge patterns, we used a recently developed quasi-geometric approach to quantify the magnitude of non-linearity of individual MU discharge patterns and the slopes of discharge rate increases

in various regions of the discharge rate profiles (Beauchamp *et al.*, 2023). In Experiment 1, we investigated the extent of MU discharge rate pattern modifications across a range of contraction levels in three different human muscles (tibialis anterior, TA; vastus lateralis and medialis, VL and VM) with special consideration for MUs that were reliably tracked across contraction levels. In Experiment 2, we investigated the extent that the duration and rate of the force increase influenced the MU discharge rate patterns during contractions at different force levels. We hypothesized that 1) estimates of PICs would increase with contraction level; 2) MU discharge rate patterns would indicate a more reciprocal pattern of inhibition with increases in contraction level; and 3) the changes in the rate of force increases and duration of contractions would have only modest effects on the contraction level-dependent effects. Our results suggest a high degree of sensitivity of neuromodulation and the pattern of inhibition with increased level of excitatory input, that is somewhat dependent on the motor pool investigated, but to a lesser extent to a change in rate of increase and duration of contraction forces.

MATERIALS AND METHODS

Participants

The study consisted of two experiments. Fifteen healthy adults participated in Experiment 1 (4 females; age: 24 ± 5 years, stature: 1.77 ± 0.08 m, mass: 71.6 ± 12.3 kg) and 11 healthy adults participated in Experiment 2 (3 females; age: 25 ± 4 years, stature: 1.77 ± 0.08 m, mass: 78.2 ± 13.8 kg). Participants had no known cardiovascular, neuromuscular, or musculoskeletal impairments, and did not take any medication known to affect the nervous system. The study was approved by Loughborough University ethics committee (2021-5361-4724) in accordance with the latest version of Declaration of Helsinki, except for registration in database. Participants provided written, informed consent prior to taking part in any experimental procedures.

Experimental design and protocol

Experiment 1

Participants visited the laboratory on three occasions, separated by at least 48 hours and no longer than 10 days. The first visit involved familiarisation with the performance of submaximal and maximal dorsiflexion and knee extension. Participants then attended two experimental sessions during which they performed isometric knee extension and dorsiflexion, respectively (randomised order). Each experimental session started with a series of warm-up submaximal isometric contractions (3 x 50, 3 x 75, and 1 x 90% of perceived maximal voluntary force; MVF). Participants then performed two to three contractions with maximal effort, separated by one minute rest, and the best trial was considered their MVF. Following determination of MVF, participants performed triangular contractions at several force levels: 15, 30, 50, and 70% of MVF. Two contractions were performed at each level. The order of contraction levels was pseudorandomised; for contractions at 15-50% MVF, the order was randomised, with the 70% MVF contractions always performed last to minimise decline in contractile function. For each contraction, participants linearly increased and decreased force to/from the target (i.e., peak) force level across 10 s in each direction (i.e., 20 s total). The contraction duration was kept constant (i.e., 20 s total) across all contraction levels, resulting in rate of force increase/decrease of 1.5, 3, 5 and 7% MVF/s respectively. To minimise MU recruitment threshold accommodation (i.e., warm-up; Gorassini et al., 2002b), at least 30, 45 and 90 seconds of rest was provided between contractions performed at 15-30, 50, and 70% MVF, respectively.

Experiment 2

Both contraction duration and rate of force increase have the capacity to alter recruitment-derecruitment hysteresis through spike-frequency adaptation and spike-threshold accommodation, respectively, as indicated by simulations (Revill & Fuglevand, 2011). Spike-frequency adaptation, which denotes a time-dependent decrease in MU discharge via inactivation of sodium channels and calcium-dependent potassium conductance (Sawczuk *et al.*, 1995; Powers *et al.*, 1999; Miles *et al.*, 2005*a*), appears to be particularly influential in contaminating the ΔF estimation, with a greater influence compared to spike-threshold accommodation (Vandenberk &

Kalmar, 2014). Thus, we prioritised standardisation of contraction duration over the rate of force increase in Experiment 1. Nevertheless, spike-frequency adaptation and spike-threshold accommodation share some of the same mechanisms; for example, sodium channel inactivation has been shown to contribute to both phenomena in rat preparations (Bradley & Somjen, 1961; Miles *et al.*, 2005*b*). To assess the potential influence of spike-threshold accommodation and spike-frequency adaptation on our results, we performed an additional experiment in the dorsiflexors. Here, participants were tasked to perform contractions of several submaximal intensities (30, 50, 70% MVF), but they did so by either performing contractions of the same duration (10 s increase/decrease, 20 s in total; rates of force increase/decrease: 3, 5, 7% MVF/s) or the same rate of force increase/decrease (5% MVF/s; total contraction durations: 12, 20, 28 seconds). Two contractions were performed per each condition and the same rest periods were employed between contractions as in Experiment 1.

Experimental procedures

Force signals

To record dorsiflexion forces, participants were seated on a custom-made chair fitted with an ankle ergometer (NEG1, OT Bioelettronica, Torino, Italy) connected to a strain gauge (CCT Transducer s.a.s., Torino, Italy), the signal of which was amplified (×200; Forza-B, OT Bioelettronica, Torino, Italy). The ankle of the dominant leg was positioned at 10° of plantar flexion (0° = anatomical position), the hip was flexed at 120° (180° = full extension) and the knee was fully extended. The foot was strapped to the dynamometer with Velcro at tarsometatarsal and metatarsal phalangeal joints. The leg was additionally strapped over the knee joint to minimise its flexion. Knee extensor force were recorded with participants seated on a custom-made isometric dynamometer with the knee and hip flexed at 115 and 125° (180° = full extension). The dominant leg was strapped (35-mm wide canvas webbing) at 15% of the tibial length in series with the strain gauge (amplification: ×370; Force Logic, Swallowfield, UK). The force signals for both dorsiflexion and knee extension were sampled at 2048 Hz and digitised with a multichannel amplifier (16-bit, Quattrocento; OT Bioelettronica, Torino, Italy).

High-density surface electromyography

High-density surface electromyograms (EMG) were recorded by placing a grid of 64 electrodes (13 rows x 5 columns, with one missing electrode; 1 mm electrode diameter, 8 mm inter-electrode distance; GR08MM1305, OT Bioelettronica, Torino, Italy) via disposable bi-adhesive foam layer (Spes Medica, Battipaglia, Italy) with its cavities filled with conductive paste (Ten20, Weaver and Company, Aurora, CO, USA) over the muscle bellies of tibialis anterior, vastus lateralis, and vastus medialis, with longitudinal axis of the electrode grid aligned with the presumed orientation of muscle fibres. The reference electrode (3M Red Dot, 3M Deutschland GmbH, Germany) was placed on the medial malleolus and the patella when recording the signals during dorsiflexion and knee extension, respectively. A dampened strap electrode was placed around the ankle of the non-dominant leg to ground the signal. The high-density EMG signals were recorded in monopolar configuration, band-pass filtered (10-500 Hz), digitised (2048 Hz) using a multichannel amplifier (16-bit, Quattrocento; OT

Bioelettronica, Torino, Italy), and acquired using OT Biolab+ software (OT Bioelettronica, Torino, Italy).

Data analysis

Force signal

In the process of off-line analysis, a 20 Hz low pass filter (4th order, zero-lag, Butterworth) was applied to the force signal to remove non-physiological properties of the signal. The force offset was removed (i.e., gravity correction) before further analysis.

High-density surface electromyography

Decomposition

Monopolar high-density surface EMG signals were initially inspected, and the channels deemed to be of poorer quality based on area under power spectrum and amplitude were removed (typically 2-3 channels). Monopolar signals were decomposed into individual MU spike trains using Convolution Kernel Compensation algorithm (Holobar & Zazula, 2007). This extensively validated algorithm inverts the EMG mixing model and estimates the separation vectors (MU filters) that represent weights of the linear spatial-temporal EMG channel combinations that yield the estimation of individual MU spike trains (Holobar *et al.*, 2010, 2014). Signals from each contraction were decomposed independently. Decomposition results were visually inspected by an experienced operator who iteratively optimised MU filters using procedures described previously (Del Vecchio *et al.*, 2020). Only the results with regular discharge patterns and/or those exhibiting the pulse-to-noise ratio ≥ 30 dB (Holobar *et al.*, 2014) were retained (accuracy >90%, false alarm rate <5%).

Motor unit tracking

We examined MU discharge patterns with and without consideration for potential MU replicates across contraction levels (see below). For the former, it was important to establish which MUs were identified across the examined contraction levels. To identify unique MUs, we used the separation vectors (MU filters), to identify MU spike trains that were common across contraction levels. The reader is referred to previously published work on the mathematical basis and validation of this approach (Francic & Holobar, 2021; Škarabot *et al.*, 2023*a*). Briefly, decomposition results of individual contractions performed at different intensities were concatenated. Considering the difficulty in identifying lower threshold MUs in the presence of much higher threshold MUs, we only concatenated contractions performed at 30, 50, and 70% MVF. In other words, we opted to exclude the trials performed at 15% MVF in this procedure as the likelihood of identifying a MU recruited during both 15 and 70% MVF was very low (Francic & Holobar, 2021). For each contraction level and individual, we selected the contraction trial with the greatest MU yield after decomposition and/or the best fit to the triangular target force. The estimated MU filters from signals obtained during one contraction were then transferred to other contractions in the concatenated signal to identify common MUs (Francic & Holobar, 2021). Since duplicate MU spike trains can

be identified when transferring MU filters, we identified those sharing 30% of the same MU discharges (discharge tolerance of 0.5 ms), and then removed them by discarding the duplicate with the lower estimated decomposition accuracy (i.e., lower pulse-to-noise ratio). As shown previously, the success of MU filter transfer varies across contraction intensities, with greater difficulty identifying discharges of lower-threshold MUs in the presence of higher-threshold MUs (Francic & Holobar, 2021). To maximise the number of tracked MUs, we therefore tracked MUs either across all concatenated contraction intensities (30-50-70% MVF) or only between neighbouring contractions (30-50 or 50-70% MVF; Figure 1).

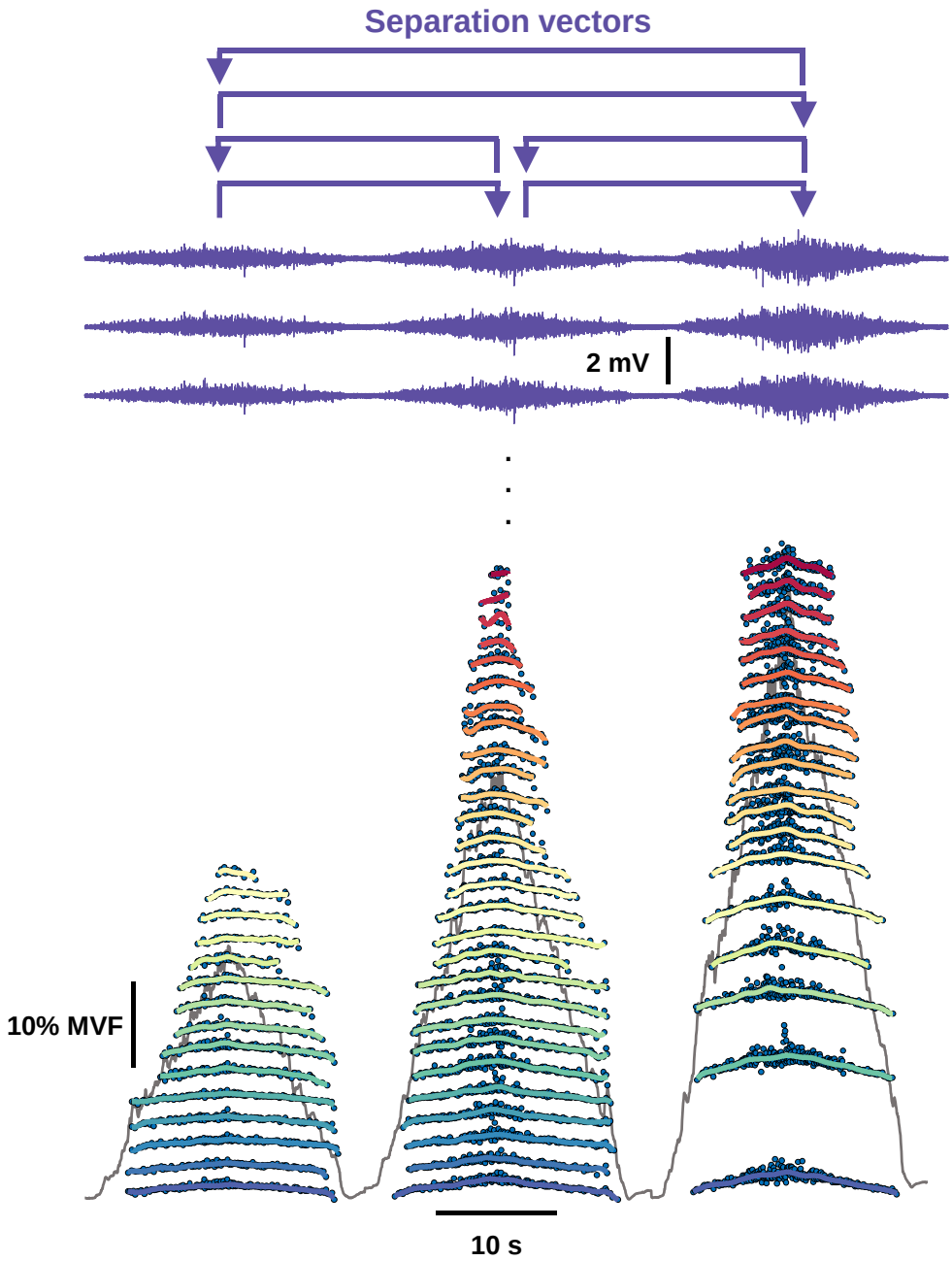

Figure 1. Identification of motor unit discharges. The approach to tracking motor units (MUs) across contraction intensities involved the estimation and application of separation vectors (MU filters) among all the possible combinations from signals obtained during contractions to 30, 50 and 70% of maximal voluntary force (MVF). Discharge patterns of tracked MUs smoothed with support vector regression are shown in colours. For clarity, only three channels of monopolar electromyography (EMG) signals are displayed.

Motor unit discharge rate metrics

Processing of motor unit spike trains. Support vector regression (SVR) was used to generate continuous estimates of MU discharge behaviour from the binary MU spike trains using procedures described previously (Beauchamp *et al.*, 2022*a*). Briefly, the instantaneous discharge rate for each MU was calculated using the reciprocal of its interspike interval, which was used to train an SVR model and generate the smooth estimates of discharge rate between recruitment and derecruitment using previously suggested parameters (Beauchamp *et al.*, 2022*a*).

Recruitment threshold and discharge rate. Recruitment and derecruitment thresholds were estimated as the instantaneous force at the instant of the first and last spike in the binary spike train, respectively. Peak discharge rate was calculated as the maximal value of the smoothed estimate of MU discharge, whereas onset and offset discharge rate were calculated as the first and last point of the SVR smoothed discharge.

Quantification of discharge rate hysteresis with respect to peak force. To quantify the discharge rate hysteresis on a single MU level, we calculated the ascending and descending duration of MU discharge with respect to peak force, and then calculated the difference in the duration of these two phases divided by the total duration of MU discharge (ascending-descending duration ratio; Figure 2A). This ratio allows the assessment of hysteresis (i.e., the amount of self-sustained discharge) with respect to force levels, with positive values indicating a leftward shift (i.e., less hysteresis) and negative values indicating a rightward shift (i.e., more hysteresis) of a single MU discharge (Hassan *et al.*, 2021).

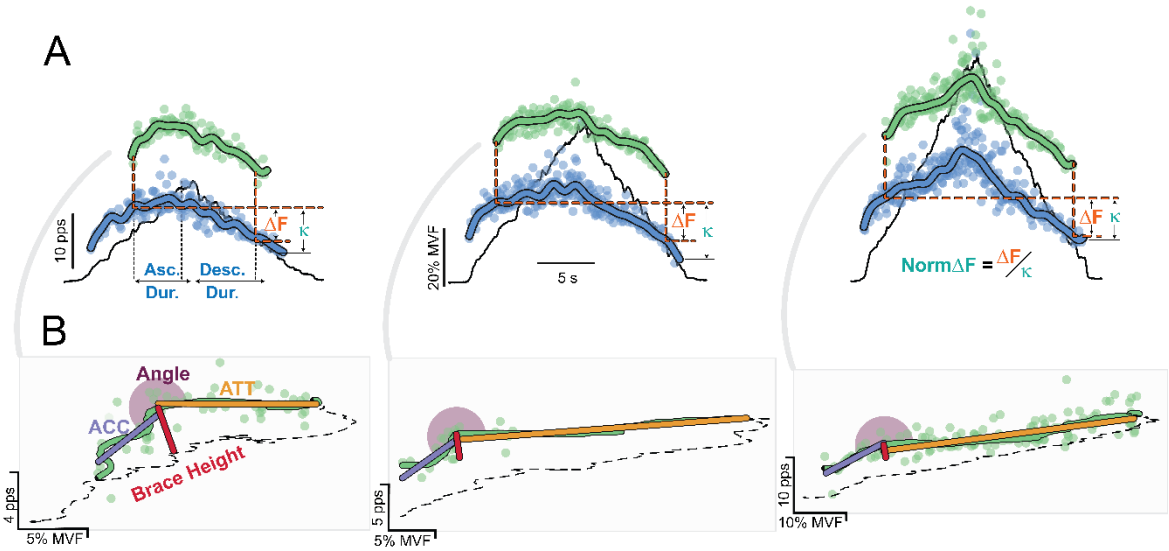

Figure 2. Analysis of motor unit discharge patterns. A: Paired motor unit (MU) analysis involved calculation of onset-offset hysteresis of a higher threshold (test) MUs with respect to a lower threshold (reporter) MU (known as ΔF). For clarity, only a pair of the same MUs across three different contraction intensities (30, 50, and 70% of maximal voluntary force; MVF) is shown. Additionally, ΔF was normalised to the theoretical maximal self-sustained discharge of the test unit (the difference between the reporter unit discharge rate at test unit recruitment and reporter unit derecruitment, κ). For each MU, the duration of discharge on the ascending and descending limb of a triangular contraction was also calculated, with the ratio denoting the hysteresis of MU discharge with respect to peak force (negative values = more hysteresis). B: Geometric analysis of single MU discharge rate with respect to force involved the calculation of brace height. The acceleration (ACC) and attenuation (ATT) slopes as well as the angle between the two slopes were also quantified.

Paired motor unit analysis. To estimate the magnitude of PICs, we calculated ΔF (Gorassini et al., 2002a; Gorassini et al., 1998), which quantifies the onset-offset hysteresis of a higher threshold (test) MU with respect to the discharge rate of a lower threshold (reporter) MU receiving common synaptic input (Figure 2A). Due to the high likelihood of many suitable reporter units for a given test unit, we calculated the average test unit ΔF for all possible reporter pairs (Hassan *et al.*, 2021; Jenz *et al.*, 2023). A pair of MUs was considered suitable if: 1) they exhibited a rate-rate correlation of $r^2 > 0.7$ (Gorassini *et al.*, 2004), to improve the likelihood that the pairs of MUs received common synaptic input; 2) the test unit was recruited at least 1 s after the recruitment of reporter unit, to ensure that PIC in the reporter unit were likely fully activated (Hassan *et al.*, 2020); and 3) the reporter unit discharge rate was >0.5 pps whilst the test unit was active, to minimise the influence of MU saturation on the calculation of ΔF (Stephenson & Maluf, 2011). Additionally, we normalised ΔF values to the difference in the reporter unit discharge rate at test unit recruitment and the discharge rate at reporter unit derecruitment, as this difference is the maximal discharge rate modulation for each test-reporter unit pair; we present this as normalised ΔF, and suggest it may be an important supplement to traditional ΔF values when reporter unit discharge rates differ vastly between contractions and/or conditions. Also note that ΔF provides an estimate of PIC magnitude but may not necessarily distinguish between the contribution of neuromodulatory drive and the amount and/or pattern of inhibitory input (Chardon *et al.*, 2022; Beauchamp *et al.*, 2023).

Geometric analysis. We used a quasi-geometric approach to estimate the deviation from linearity in MU discharge rate with respect to force output, which we previously refer to as brace height (Figure 2B; Beauchamp et al., 2023). Briefly, the smoothed discharge rate of a single MU was expressed as a function of force produced during a contraction, and the maximum orthogonal vector between this smoothed discharge and a theoretical linear increase in discharge from MU recruitment to peak was quantified. The absolute magnitude of this maximum orthogonal vector is then termed brace height. To ensure that brace height quantifies a relative deviation of discharge patterns from linearity, and to remove potential confounds with changes in peak discharge, we normalised brace height values to the height of a right triangle with a hypotenuse between recruitment and peak MU discharge. MUs with a negative slope of the acceleration phase, normalised brace height greater than 200%, or with peak MU discharge rate occurring after peak force were excluded from further analysis. The estimation of brace height has been shown to be highly sensitive to changes in neuromodulatory drive in motoneuron simulations (Chardon *et al.*, 2022; Beauchamp *et al.*, 2023).

In addition to brace height, we calculated the slope of the initial acceleration phase of MU discharge, the subsequent attenuation phase of MU discharge, and the angle between the two phases (Beauchamp *et al.*, 2023). The slopes of these two phases correspond to the secondary and tertiary range of MU discharge. The secondary range represents an abrupt increase in MU discharge rate following recruitment, likely due to PIC activation (Li *et al.*, 2004), which is followed by attenuated MU discharge rate increase (tertiary range) as the PIC conductance is increased and the potassium currents are activated (Li & Bennett, 2007). The attenuation phase of the MU discharge has been shown to be particularly influenced by the *pattern* of local inhibition (Powers *et al.*, 2012; Beauchamp *et al.*, 2023) and may thus, in combination with brace height and ΔF metrics, allow for us to uncouple the contributions of neuromodulatory

and inhibitory inputs to MU discharge patterns. Conversely, acceleration phase slope and the angle between acceleration and attenuation phases have been shown to be relatively insensitive to patterns of inhibitory inputs in a simulation study (Beauchamp *et al.*, 2023). However, delivering inhibitory cutaneous stimuli has previously been shown to linearise MU discharge profiles in humans (Revill & Fuglevand, 2017). Thus, rather than the pattern of inhibition, the angle between acceleration and attenuation phases is likely to be sensitive to the total inhibitory input, i.e., increased inhibitory input could lead to smaller angles.

Ensemble averaging. To provide a visual comparison of MU behaviour across different contraction levels, we constructed ensemble averages of all MUs identified across participants for each contraction level and muscle (Beauchamp *et al.*, 2022*a*). Identified MUs were separated into bins according to their recruitment threshold and the discharge patterns of MUs were smoothed with SVR as detailed above. The discharge behaviour of each MU was then normalized in time according to the average discharge duration within each ensemble cohort. This normalisation procedure involved adjusting sampling rates of the prediction vectors as to equalise the length of all smoothed MU discharges within an ensemble with respect to the average length of the time vector between MU recruitment and derecruitment sampled at 2048 samples per second. Note that this approach is relevant only for the purposes of visual representation of MU behaviour and was not used when calculating any MU discharge metrics or for statistical comparisons.

Statistical analyses

To assess changes in MU discharge characteristics across contraction level, we fit a linear mixed effects model to each MU discharge metric. The model consisted of contraction level, muscle and their interaction as fixed effects and participant and trial (i.e., repeat trials) as random intercepts. Additionally, since decomposition is biased towards discriminating higher-threshold MUs in each context/contraction level (Farina *et al.*, 2010), and because proportions of the motor pool with moderate recruitment thresholds are likely to have been sampled across all of our contraction levels, we employed MU recruitment threshold as a covariate in our model. For example, to assess how ΔF is modulated across contraction levels in Experiment 1, our model was as follows: ΔF ~ Contraction Level*Muscle + Recruitment Threshold + [1 | Participant ID] + [1 | Trial]. For the analyses in Experiment 2 we replaced the fixed effect of ‘muscle’ with the fixed effect of ‘condition’ in our model to denote whether the contractions were performed with matched duration or matched rate of force increase. Because the 50% MVF condition was the same for both rate- and duration-matched contractions, we randomly assigned one trial at 50% to either the rate- or duration-matched condition. When assessing the change in outcome metrics across contraction level for tracked MUs, we further considered the nesting of a particular set of tracked MUs within a given participant (e.g., peak discharge rate ~ Contraction Level*Muscle + Recruitment Threshold + [1 | Participant ID] + [1 | Matched MU ID: Participant ID]). For ΔF data, rather than nesting of tracked MUs, we considered nesting of reporter and test units within a participant as random intercepts, as well as the recruitment threshold of test and reporter units as covariates (e.g., ΔF ~ Contraction Level*Muscle + reporter MU threshold + test MU threshold + [1 | Participant ID] + [1 | reporter MU ID: Participant ID] + [1 | test MU ID: Participant ID]).

All analyses were performed in R (R studio, v 1.4.1106, R Foundation for Statistical Computing, Vienna, Austria). Linear mixed effect models were constructed with *lme4* package (Bates *et al.*, 2015). The significance of the model was assessed by comparing the fit of the model with and without the predictor variables using *lmerTest* package (Kuznetsova *et al.*, 2017). The assumptions of normality, linearity and homoscedasticity of residuals were assessed using quantile-quantile plots and histograms. For significant main effects or interactions, post hoc testing of estimated marginal means with Tukey adjustments for multiple comparisons was performed using *emmeans* package (Lenth & Lenth, 2018). Residuals of predictions were found to be non-linear for the following variables: peak discharge rate (log-transformed), discharge rate at recruitment and derecruitment (sqrt-transformed), normalised ΔF (sqrt-transformed), acceleration slope (log), and attenuation slope (log) for non-tracked analysis, and peak discharge rate (log), ascending/descending ratio (sqrt), and acceleration and attenuation slopes (both log) for tracked unit analysis in Experiment 1. For analysis of Experiment 2, the residuals of following variables were found to be non-linearly distributed: ascending/descending ratio (sqrt), acceleration (log), and attenuation (log) for non-tracked MU data, and peak discharge rates (log), normalised ΔF (sqrt), ascending/descending ratio (sqrt), acceleration (log) and attenuation (log) for tracked MU data. In the aforementioned cases, data were transformed for the linear mixed model, and then back transformed when calculating estimated marginal means.

We performed additional exploratory analyses to assess the relationship between the peak discharge rate and the recruitment threshold of a given MU across different contraction levels and in different muscles. For this analysis, only MUs tracked across 30, 50 and 70% of MVF were used. In the case of TA, data was pooled for unique participants in Experiment 1 and the duration-matched condition in Experiment 2. We then calculated the repeated measures correlation coefficient separately for each contraction level and muscle using *rmcorr* package (Bakdash & Marusich, 2017). In all cases, significance was set at an alpha level of 0.05.

RESULTS

Motor unit identification

In experiment 1, we identified a total of 1930, 1064, and 600 MUs for tibialis anterior (n = 15 participants, 4 female), vastus lateralis (n = 15 participants, 4 female) and medialis (n = 12 participants, 1 female) across all contractions, respectively. Note that the number of participants differs for vastus medialis because we were not able to identify any units in 3 participants (all female) from the signals obtained from this muscle. When considering tracked MUs by estimating and applying MU filters, we were able to identify 86 unique MUs across all three contraction levels (30, 50 and 70%) in tibialis anterior in 12 individuals, 35 MUs in vastus lateralis, and 18 MUs for vastus medialis. A greater number of units were identified when considering either 30 and 50%, or 50 and 70% MVC contractions (Table 1).

In Experiment 2, we identified 1018 and 932 MUs in the duration-matched and rate-matched conditions, respectively. When tracked across contraction levels, we identified 74 and 60 unique MUs across 30, 50, and 70% MVF in the duration-matched and rate-matched conditions, respectively (Table 1).

Table 1. The number of identified motor units from decomposition. Values denote the mean number of identified motor units (standard deviation) per participant. TA = tibialis anterior, VL = vastus lateralis, VM = vastus medialis.

	Experiment 1		
	All motor units		
	TA *[n = 15]*	***VL*** *[n = 14]*	***VM*** *[n = 12]*
15% MVF	19.1 (6.1)	11.5 (6.6)	6.8 (2.4)
30% MVF	17.9 (6.2)	10.1 (6.8)	6.1 (3.0)
50% MVF	15.2 (5.5)	8.5 (6.9)	6.1 (3.5)
70% MVF	14.0 (6.2)	7.1 (5.1)	6.3 (4.4)
sum	1930	1064	600
	Tracked motor units		
	TA	***VL***	***VM***
30-50-70% MVF	7.2 (4.6); n = 12	4.5 (4.3); n = 8	3.0 (4.0); n = 6
30-50% MVF	14.2 (5.9); n = 15	8.6 (8.7); n = 13	4.8 (4.0); n = 9
50-70% MVF	13.8 (6.8); n = 13	7.3 (7.3); n = 14	6.7 (4.8); n = 10

	Experiment 2	
	All motor units	
	Matched – duration *[n = 11]*	***Matched – rate*** *[n = 11]*
30% MVF	24.0 (10.9)	20.0 (9.5)
50% MVF	18.1 (8.3)	16.9 (8.0)
70% MVF	13.2 (7.0)	14.0 (7.2)
sum	1018	932
	Tracked motor units	
	Matched – duration	***Matched – rate***
30-50-70% MVF	7.4 (3.5); n = 10	6.7 (4.6); n = 9
30-50% MVF	14.3 (7.6); n = 11	12.3 (7.4); n = 11
50-70% MVF	11.9 (5.7); n = 11	12.4 (7.0); n = 11

Experiment 1

To appreciate the discharge patterns of all identified MUs across participants for each muscle, we represented MUs in ensemble averages. For each muscle, the discharge patterns of all MUs were smoothed with SVR and separated into ten equally spaced bins as a function of recruitment threshold. The ensemble averages for each muscle and across all contraction levels are shown in Figure 3A, along with the mean force profile and the cumulative spike trains across all participants. Because results were similar when assessing the discharge behaviour of all units as well as those units that were tracked, we only present the latter below. The results of all, i.e., non-tracked, units for both experiments are presented in the Supplementary Material.

As can be appreciated in Figure 3A, peak discharge rates were predicted by contraction level ($\chi^2(2) = 2259.4$, $p < 0.0001$), muscle ($\chi^2(2) = 2248.9$, $p < 0.0001$), and recruitment threshold ($\chi^2(1) = 278.1$, $p < 0.0001$). In all muscles, peak discharge rates increased with greater contraction level ($p < 0.0001$). There was also a significant interaction between contraction level and muscle ($\chi^2(4) = 18.3$, $p = 0.0011$), such that during contractions at the same relative force level TA peak discharge rates were greater than VL and VM ($p < 0.0001$; Figure 3B). The discharge rate at recruitment (Figure 3D) was also influenced by contraction level ($\chi^2(2) = 19.0$, $p < 0.0001$), muscle ($\chi^2(2) = 219.2$, $p < 0.0001$), and recruitment threshold ($\chi^2(1) = 67.3$, $p < 0.0001$), but there was no interaction between contraction level and muscle ($\chi^2(4) = 9.5$, $p = 0.0507$). At derecruitment (Figure 3E), discharge rate was also predicted by contraction level ($\chi^2(2) = 7.2$, $p = 0.0272$), muscle ($\chi^2(2) = 262.4$, $p < 0.0001$), and recruitment threshold ($\chi^2(1) = 133.8$, $p < 0.0001$), and there was also a significant interaction between the contraction level and muscle ($\chi^2(4) = 11.4$, $p = 0.0229$).

When considering untracked MUs, there was a tendency for less hysteresis of a single MU discharge with respect to peak force levels with greater contraction level (Supplementary Material), but this was seemingly not the case when observing the behaviour of the same units across different contraction levels. Indeed, ascending/descending ratio was predicted by contraction level ($\chi^2(2) = 38.7$, $p < 0.0001$), and recruitment threshold ($\chi^2(1) = 177.1$, $p < 0.0001$), but not muscle ($\chi^2(2) = 3.0$, $p = 0.2239$). In VL, ascending/descending duration ratio decreased with contraction level ($p \leq 0.0180$), whereas in TA and VM ascending/descending duration was similar during 30 and 50% MVF ($p = 0.9999$ and $p = 0.2628$, respectively), but was smaller at 70% compared to lower contraction levels ($p < 0.0001$ for both; Figure 3C) indicating greater hysteresis, or sustained discharge whilst performing contractions to higher force levels.

ΔF was predicted by contraction level ($\chi^2(2) = 555.9$, $p < 0.0001$), muscle ($\chi^2(2) = 1252.5$, $p < 0.0001$), and their interaction ($\chi^2(4) = 262.1$, $p < 0.0001$). Furthermore, ΔF was also predicted by the recruitment threshold of test ($\chi^2(1) = 397.9$, $p < 0.0001$) and reporter unit ($\chi^2(1) = 6.7$, $p < 0.0001$). In TA, ΔF increased as a function of contraction level ($p < 0.0001$). In VL, there was a decrease observed in ΔF between 30 and 50% ($p < 0.0001$), but then increased at 70% ($p < 0.0001$), which was also greater compared to 30% MVF ($p = 0.0239$). In VM, ΔF was greater at 70% compared to 30% MVF ($p = 0.0152$). The ΔF values were greater in TA at all relative contraction levels compared to VL and VM ($p < 0.0001$), whereas differences between VL and VM were only evident at 50% ($p = 0.0015$; Figure 3F).

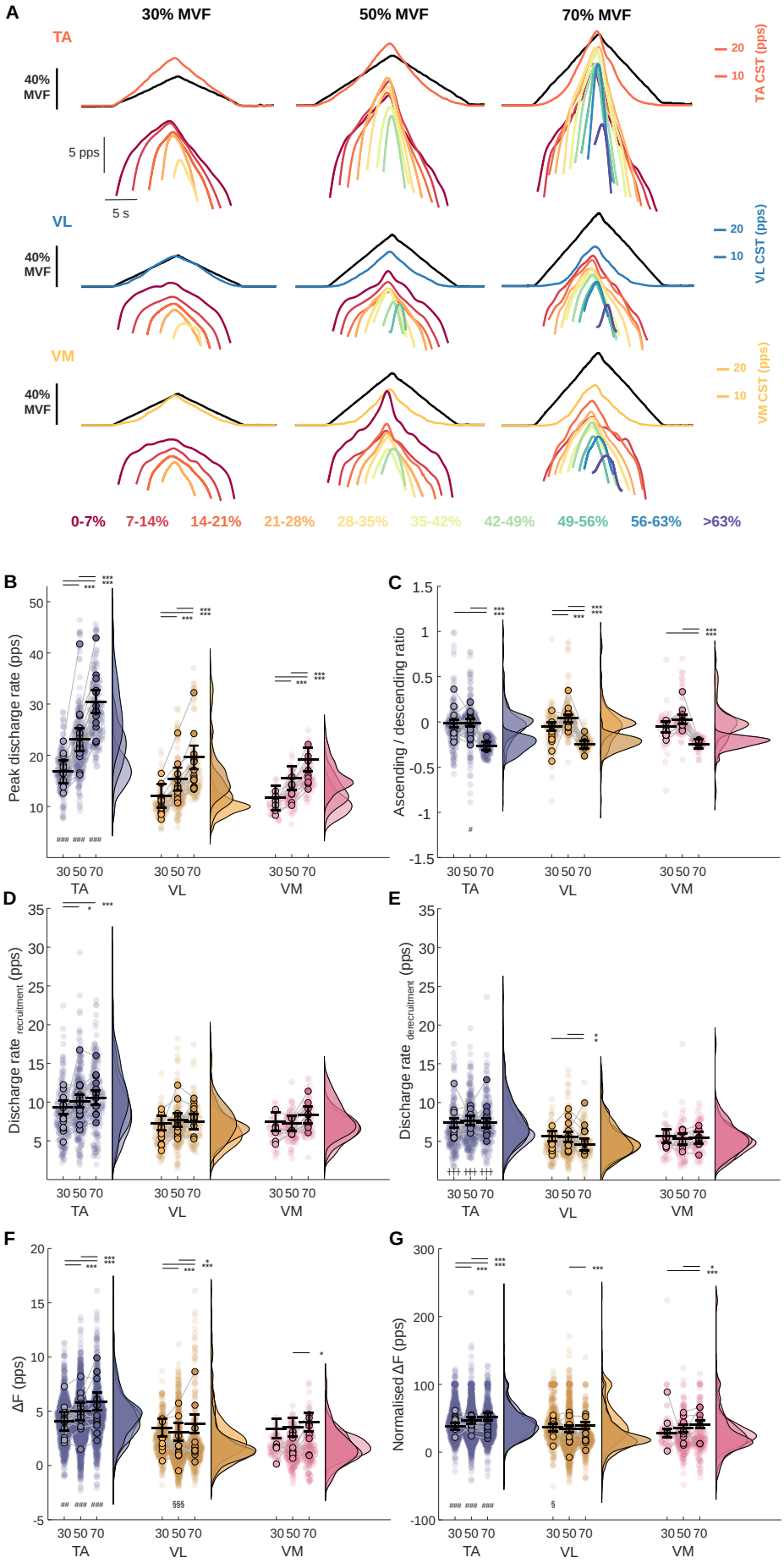
A
30% MVF
50% MVF
70% MVF
TA
VL
VM
40% MVF
5 pps
5 s
TA CST (pps)
VL CST (pps)
VM CST (pps)
0-7%
7-14%
14-21%
21-28%
28-35%
35-42%
42-49%
49-56%
56-63%
>63%
B
Peak discharge rate (pps)
C
Ascending / descending ratio
D
Discharge rate recruitment (pps)
E
Discharge rate derecruitment (pps)
F
ΔF (pps)
G
Normalised ΔF (pps)
TA
VL
VM

Figure 3. Discharge rate modulation and hysteresis as a function of contraction level and muscle. A: Ensemble averages of motor unit discharge patterns based on recruitment threshold in 7% MVF bins (colour-coded) along with the ensemble force profiles (black) and cumulative spike trains in tibialis anterior (TA), vastus lateralis (VL), and vastus medialis (VM), during triangular contractions up to 30, 50 and 70% of maximal voluntary force (MVF). B: Peak discharge rates (in pulses per second, pps) obtained as the maximal value of motor unit discharge patterns smoothed with support vector regression. C: the ratio of the ascending and descending phase of motor unit discharge rate with respect to peak force levels as an estimate of self-sustained motor unit discharge (positive values indicate less hysteresis). D: Discharge rate at motor unit recruitment. E: Discharge rate at motor unit derecruitment. F: Estimation of the onset-offset hysteresis (ΔF) between a pair of motor units that share a high proportion of common synaptic input. G: ΔF as in D but normalised to the to the difference in the reporter unit discharge rate at test unit recruitment and the discharge rate at reporter unit derecruitment. In B-G, the coloured circles represent individual participant averages, the opaque circles denote values of individual motor units with their kernel density distribution also plotted. The horizontal black lines denote the estimated marginal means obtained from the linear mixed statistical modelling with the error bars denoting a 95% confidence interval. ***$p < 0.001$, **$p < 0.01$, *$p < 0.05$ relative to other contraction levels, $^{\#\#\#}p < 0.001$, $^{\#\#}p < 0.01$, $^{\#}p < 0.01$ relative to VL and VM at the same force level; $^{\S\S\S}p < 0.001$, $^{\S\S}p < 0.01$, $^{\S}p < 0.05$ relative to VM at the same force level; $^{+++}p < 0.001$ compared to VL at the same force level.

Similarly, the normalised ΔF was predicted by contraction level ($\chi^2(2) = 44.7$, $p < 0.0001$), muscle ($\chi^2(2) = 523.3$, $p < 0.0001$), and their interaction ($\chi^2(4) = 136.2$, $p < 0.0001$), as well as recruitment threshold of test ($\chi^2(1) = 1056.0$, $p < 0.0001$) and reporter units ($\chi^2(1) = 126.9$, $p < 0.0001$). The post hoc testing indicated similar results to the absolute ΔF, with an increase in normalised values as a function of contraction level in TA ($p < 0.0001$). In VL, normalised ΔF was greater during contractions to 70% compared to 50% ($p = 0.0005$), whereas in VM similar ΔF values were observed between 30 and 50% ($p = 0.1160$), but then increased when contractions were performed to 70% ($p = 0.0307$; Figure 3G).

The modulation in discharge rate in the TA with respect to force output during different contraction levels can be appreciated in Figure 4A. The quasi-geometric analysis of tracked units indicated a tendency for more linear discharge patterns with contractions performed at greater force levels. Brace height, an indicator of non-linearity, was predicted by contraction level ($\chi^2(2) = 143.2$, $p < 0.0001$) and recruitment threshold ($\chi^2(1) = 26.6$, $p < 0.0001$), but not muscle ($\chi^2(2) = 2.3$, $p = 0.3121$). There was an interaction between contraction level and muscle ($\chi^2(4) = 24.9$, $p < 0.0001$). In TA, brace height decreased as a function of contraction level ($p \leq 0.0292$). In VL, brace height decreased from 30% to 50% ($p < 0.0001$) but then remained similar between 50 and 70% MVF ($p = 1.0000$), whereas in VM the only observed difference was between 30 and 70% MVF with brace height being smaller during the latter ($p = 0.0046$; Figure 4B). The tendency for discharge rate patterns to become more linear at higher force levels was further supported by the results of the angle between acceleration and attenuation slopes, which was predicted by contraction level ($\chi^2(2) = 204.9$, $p < 0.0001$), muscle ($\chi^2(2) = 73.3$, $p < 0.0001$), and recruitment threshold ($\chi^2(1) = 278.1$, $p < 0.0001$). There was also a significant interaction between contraction level and muscle ($\chi^2(4) = 21.2$, $p = 0.0003$). The angle decreased as a function of contraction level in TA ($p \leq 0.0073$) and VM ($p \leq 0.0425$), whereas in VL there were no differences between contractions at 50 and 70% MVF ($p = 0.0575$; Figure 4C).

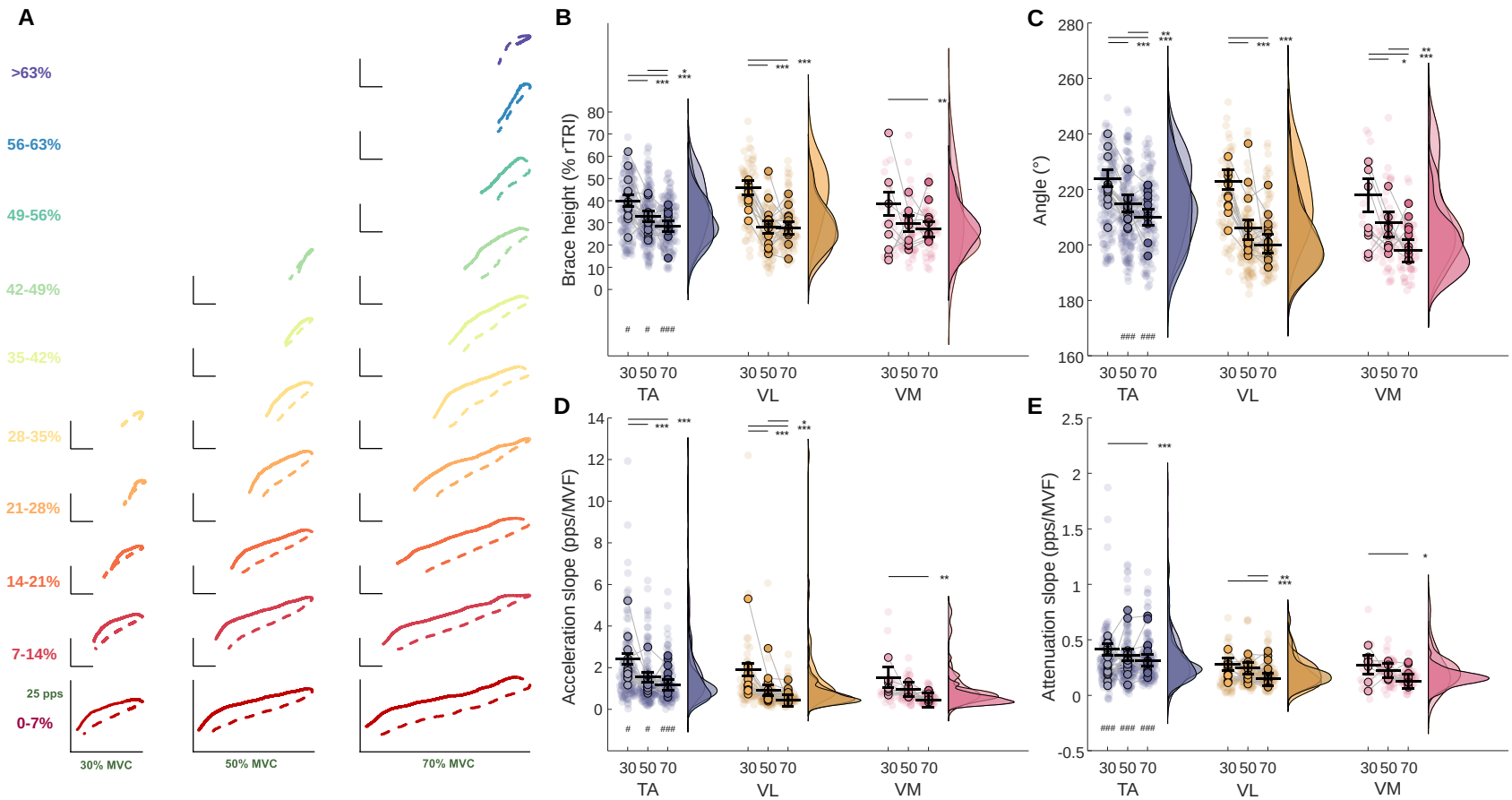

Figure 4. Geometric analysis of discharge rate modulation as a function of contraction level and muscle. A: Ensembles of tibialis anterior (TA) motor unit discharge (pulses per second, pps) increase (full lines) and decrease (dashed lines) as a function of a change in dorsiflexion force during 30 (left column), 50 (middle column), and 70% (right column) of MVF contractions. Each colour represents an ensemble of motor unit discharges stratified by recruitment thresholds in 7% MVF bins. B: Brace height expressed as a percentage of a right triangle (% rTRI) in TA, vastus lateralis (VL) and medialis (VM). C: The angle between the acceleration and attenuation slopes. D: the acceleration slope. E: the post-acceleration attenuation slope. The coloured circles represent individual participant averages, the opaque circles denote values of individual motor units with their kernel density distribution also plotted. The horizontal black lines denote the estimated marginal means obtained from the linear mixed statistical modelling with the error bars denoting a 95% confidence interval. ***$p < 0.001$, **$p < 0.01$, *$p < 0.05$ relative to other contraction levels, $^{###}p < 0.001$, $^{##}p < 0.01$, $^{#}p < 0.01$ relative to VL and VM at the same force level.

The acceleration slope was predicted by contraction level ($\chi^2(2) = 214.1$, $p < 0.0001$), muscle ($\chi^2(2) = 129.6$, $p < 0.0001$), recruitment threshold ($\chi^2(1) = 111.4$, $p < 0.0001$), as well as contraction level and muscle interaction ($\chi^2(4) = 14.4$, $p < 0.0001$). In VL, acceleration slope decreased with greater contraction levels ($p \leq 0.0465$), whereas it also decreased between 30 and 50% for TA ($p < 0.0001$), but not 50 and 70% MVF ($p = 0.0795$). In VM, the only difference was noted between 30 and 70% ($p = 0.0027$; Figure 4D). The attenuation slope was also predicted by contraction level ($\chi^2(2) = 46.5$, $p < 0.0001$), muscle ($\chi^2(2) = 141.7$, $p < 0.0001$), and recruitment threshold ($\chi^2(1) = 92.0$, $p < 0.0001$). In TA and VM, the only difference in attenuation slope was noted between 30 and 70% MVF ($p = 0.0001$ and $p = 0.0287$, respectively). In VL, the attenuation slopes were similar at 30 and 50% MVF ($p = 0.9404$), but then decreased between 50 and 70% ($p = 0.0018$; Figure 4E).

Experiment 2

Subtle differences in MU discharge patterns across contraction levels matched for either the contraction duration or the rate of force increase can be appreciated in the ensemble averages in Figure 5A. Note that the 50% contractions are equivalent for both duration- and rate-matched contractions.

When considering MUs tracked across contraction levels either during duration- or rate-matched contractions, peak discharge rates were predicted by contraction level ($\chi^2(2) = 2867.4$, $p < 0.0001$), and recruitment threshold ($\chi^2(1) = 97.5$, $p < 0.0001$), but not condition ($\chi^2(1) = 2.1$, $p = 0.1490$). In both conditions, peak discharge rates increased with greater contraction level ($p < 0.0001$; Figure 5B). The discharge rate at motor unit recruitment was predicted by contraction level ($\chi^2(2) = 21.1$, $p < 0.0001$), and recruitment threshold ($\chi^2(1) = 58.1$, $p < 0.0001$), but not condition ($\chi^2(1) = 0.1$, $p = 0.9663$). There was also an interaction between contraction level and condition ($\chi^2(2) = 9.4$, $p = 0.0090$), though post hoc testing did not reveal any differences between conditions at the same relative force levels (Figure 5C). Discharge rate at motor unit derecruitment was also predicted by contraction level ($\chi^2(2) = 9.7$, $p = 0.0079$), and recruitment threshold ($\chi^2(1) = 98.0$, $p < 0.0001$), but was not influenced by condition ($\chi^2(1) = 0.9$, $p = 0.3310$; Figure 5D).

The ascending/descending duration ratio was predicted by contraction level ($\chi^2(2) = 28.5$, $p < 0.0001$), condition ($\chi^2(1) = 10.2$, $p = 0.0014$), recruitment threshold ($\chi^2(1) = 111.9$, $p < 0.0001$), as well as contraction level and muscle interaction ($\chi^2(2) = 7.4$, $p = 0.0065$). For rate-matched contractions, ascending/descending duration decreased with increased contraction level ($p \leq 0.0084$), whereas for duration-matched there was an overall reduction in the ascending/descending duration with contraction level but no difference between 30 and 50% MVF ($p = 0.1198$; Figure 5E).

ΔF was predicted by contraction ($\chi^2(2) = 554.9$, $p < 0.0001$), but not condition ($\chi^2(1) = 3.3$, $p = 0.06866$). Main effects were also noted for recruitment threshold of test ($\chi^2(1) = 73.8$, $p < 0.0001$) and reporter ($\chi^2(1) = 108.2$, $p < 0.0001$) units, and there was an interaction between contraction level and condition ($\chi^2(2) = 64.8$, $p < 0.0001$). In both conditions, ΔF increased with greater contraction level ($p < 0.0001$). During duration-matched contractions, ΔF was greater compared to rate-matched contractions at 30% ($p < 0.0001$), but similar at 50% ($p = 0.7222$) and 70% MVF ($p = 0.7365$; Figure 5F). When normalised, ΔF was similarly predicted by contraction ($\chi^2(1) = 436.2$, $p < 0.0001$), and recruitment threshold of the test ($\chi^2(1) = 567.6$, $p < 0.0001$) and reporter

unit ($\chi^2(1) = 275.9$, $p < 0.0001$), but not condition ($\chi^2(1) = 2.1$, $p = 0.1469$). There was also a significant interaction between contraction and condition ($\chi^2(2) = 8.3$, $p = 0.0158$). The normalised ΔF increased with greater contraction level ($p < 0.0001$); but the values were greater at 30% MVF for the duration-matched condition ($p = 0.0181$; Figure 5G).

Brace height was predicted by contraction level ($\chi^2(2) = 216.4$, $p < 0.0001$) and recruitment threshold ($\chi^2(1) = 49.4$, $p < 0.0001$), but not condition ($\chi^2(2) = 3.5$, $p = 0.0629$). There was an interaction between contraction level and muscle ($\chi^2(2) = 11.2$, $p = 0.0038$). In duration-matched contractions, brace height decreased with greater contraction level ($p < 0.0001$), whereas, although it was reduced at 70%, it was similar between 30 and 50% MVF for rate-matched contractions ($p = 0.0503$; Figure 5H).

The angle between acceleration and attenuation slopes was predicted by contraction level ($\chi^2(2) = 183.9$, $p < 0.0001$) and recruitment threshold ($\chi^2(1) = 94.3$, $p < 0.0001$), but not by condition ($\chi^2(1) = 2.8$, $p = 0.0923$). However, there was a significant interaction between contraction and condition ($\chi^2(2) = 41.8$, $p < 0.0001$). In duration-matched contractions, the angle decreased as a function of contraction level ($p < 0.0001$), whereas during rate-matched contractions, the angle was similar at 30 and 50% MVF ($p = 0.9310$). At 30% MVF, the angle was greater for longer contractions ($p < 0.0001$; Figure 5I).

Acceleration slope was predicted by contraction level ($\chi^2(2) = 106.0$, $p < 0.0001$) and recruitment threshold ($\chi^2(1) = 84.2$, $p < 0.0001$), but not condition ($\chi^2(2) = 2.6$, $p = 0.1077$). A significant interaction between contraction level and interaction was also observed ($\chi^2(2) = 41.7$, $p < 0.0001$). In duration-matched contractions, acceleration slope decreased with greater contraction level, whereas they were only smaller during 70% compared to 30% MVF for the rate-matched contraction ($p = 0.0132$; Figure 5H). The acceleration slope was also greater during duration-matched compared to rate-matched at 30% MVF ($p < 0.0001$; Figure 5J), indicating that PIC activation played a larger role in the initial discharge rate increases during slow rates of force increase. Attenuation slope was predicted by contraction level ($\chi^2(2) = 25.2$, $p < 0.0001$) and recruitment threshold ($\chi^2(1) = 80.7$, $p < 0.0001$), but not condition ($\chi^2(1) = 0.1$, $p = 0.8185$; Figure 5K).

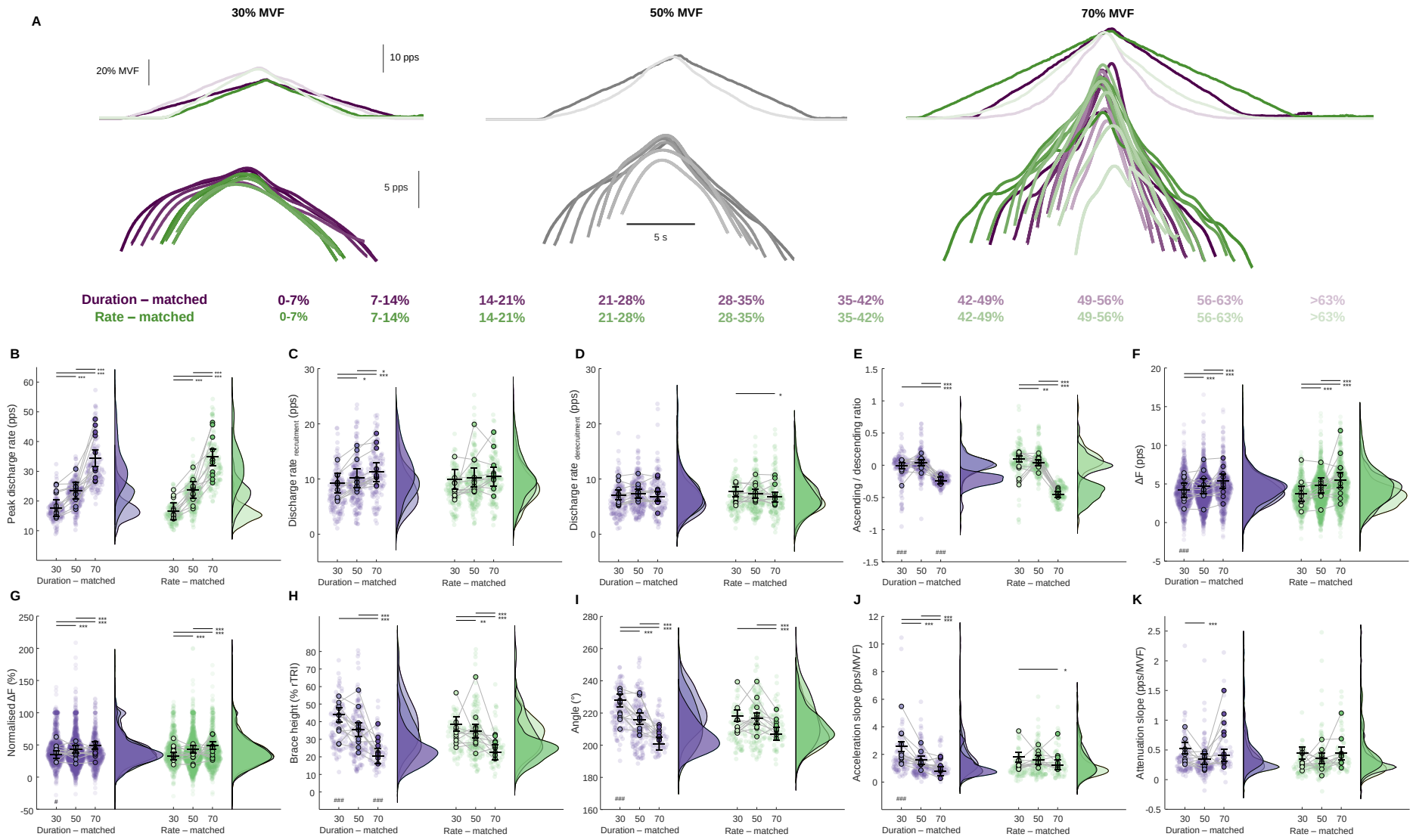

Figure 5. Discharge rate modulation in tracked motor units across contraction forces matched for contraction duration or rate of force increase. A: Ensemble averages of tibialis anterior motor unit discharge patterns based on recruitment threshold in 7% MVF bins (coded by the colour opacity) along with the ensemble force

profiles (black) and cumulative spike trains during triangular contractions up to 30, 50 and 70% of maximal voluntary force (MVF) matched for either contraction duration or rate of force rise. B: Peak discharge rates (in pulses per second, pps) obtained as the maximal value of motor unit discharge patterns smoothed with support vector regression. C: Discharge rate at motor unit recruitment. D: Discharge rate at motor unit derecruitment. E: the ratio of the ascending and descending phase of motor unit discharge rate with respect to peak torque levels as an estimate of self-sustained motor unit discharge (positive values indicate less hysteresis). F: Estimation of the onset-offset hysteresis (ΔF) between a pair of motor units that share a high proportion of common synaptic input. G: ΔF as in D, but normalised to the to the difference in the reporter unit discharge rate at test unit recruitment and the discharge rate at reporter unit derecruitment. H: Brace height expressed as a percentage of the right triangle. I: The angle between the acceleration and attenuation slopes. J: the acceleration slope. K: the post-acceleration attenuation slope. In B-K, the coloured circles represent individual participant averages, the opaque circles denote values of individual motor units with their kernel density distribution also plotted. The horizontal black lines denote the estimated marginal means obtained from the linear mixed statistical modelling with the error bars denoting a 95% confidence interval. ***$p < 0.001$, **$p < 0.01$, *$p < 0.05$ relative to other contraction levels, $^{###}p < 0.001$, $^{##}p < 0.01$, $^{#}p < 0.01$ relative to the other condition at the same force level.

Exploratory analysis – the relationship between recruitment threshold and peak discharge rate

In TA, the relationship between peak MU discharge rates and recruitment threshold of MUs was significantly negative during contractions performed up to 30% (r_m = -0.43 [-0.57, -0.26], p < 0.0001), indicating that the recruitment threshold and discharge rate patterns followed an onion skin pattern. When performing contractions up to 50% MVF, no relationship was demonstrated between peak discharge rates and recruitment threshold (r_m = 0.08 [-0.10, 0.26], p = 0.3800), which likely indicates a convergence of the peak discharge rates of MUs of various recruitment thresholds. At 70% MVF, the relationship turned significantly positive (r_m = 0.20 [0.02, 0.37], p = 0.0336; Figure 6A), indicating that higher threshold MUs were discharging at higher rates than lower threshold units (i.e., inverse onion skin; Inglis & Gabriel, 2021). In VM, peak MU discharge rates were negatively associated with recruitment threshold across all contraction levels (30%: r_m = -0.86 [-0.96, -0.60], p = 0.0001; 50%: r_m = -0.90 [-0.97, -0.68], p < 0.0001; 70%: r_m = -0.82 [-0.95, -0.50], p = 0.0006; Figure 6C), whereas in VL this was the case during contraction up to 30% (r_m = -0.66 [-0.83, -0.39], p = 0.0001) and 50% (r_m = -0.59 [-0.79, -0.28], p = 0.0009), but no significant relationship was evident during 70% MVF (r_m = -0.35 [-0.64, 0.02], p = 0.0639; Figure 6B). Note that in this analysis, MU discharges were tracked across different contraction levels, so the relationships reflect the behaviour of only those MUs with a recruitment threshold of up to 30% MVF.

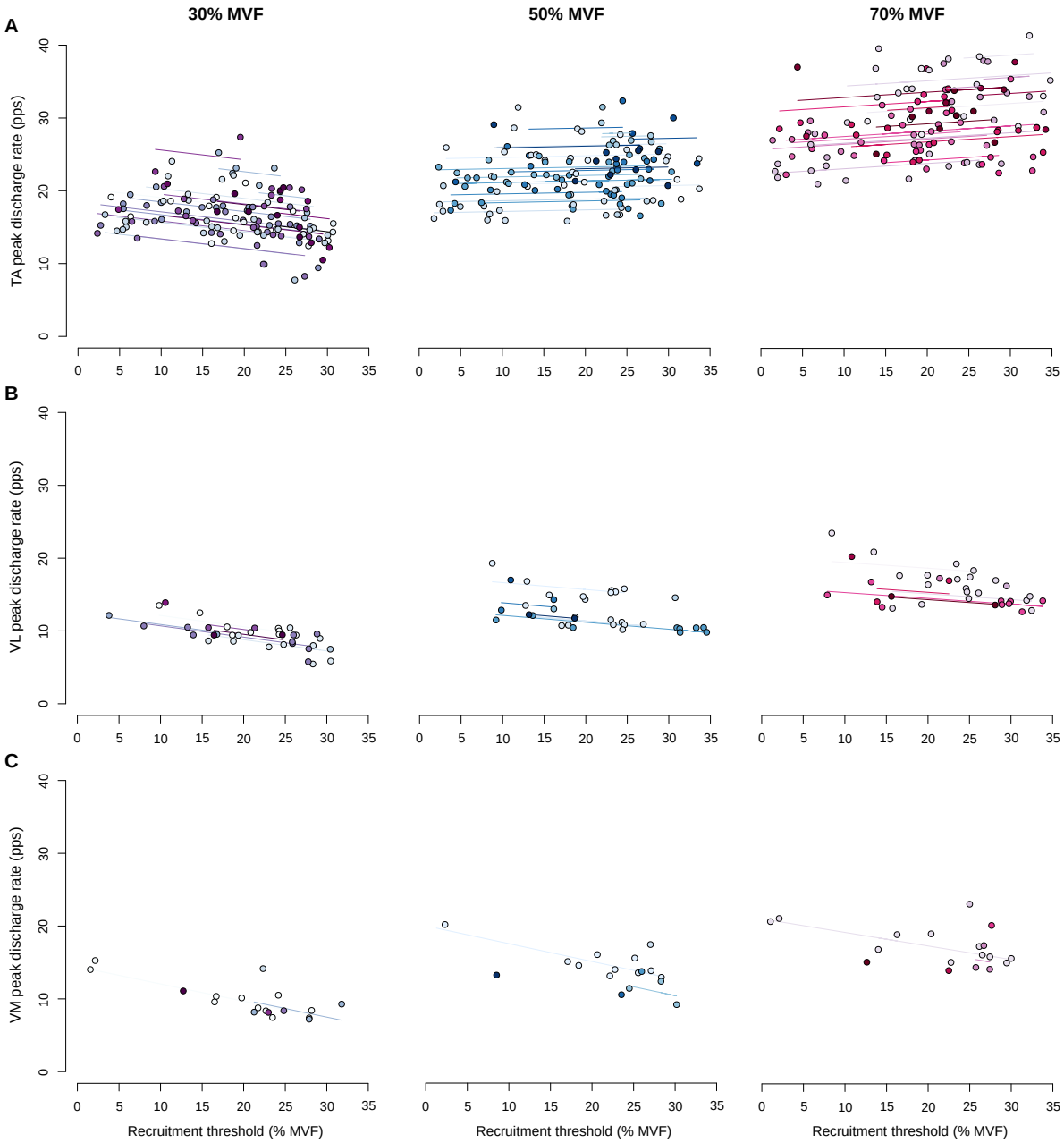

Figure 6. The relationship between recruitment threshold and peak discharge rates of motor units across different contraction levels and muscles. The analysis was performed by calculating the repeated measures correlation coefficient (indicated by coloured lines) only on motor units tracked across triangular contractions up to 30, 50 and 70% of maximal voluntary force (MVF). For visual purposes only, the black lines indicate the regression if all units are considered equally.

DISCUSSION

Leveraging the high yield of MU discharge patterns identified from decomposition of multichannel EMG recordings, we show that neuromodulation and patterns of inhibition are uniquely shaped to support the need for greater contraction force across a large proportion of the motor pool's recruitment range in three human lower limb muscles. In particular, our results suggest that the *relative* contribution of PICs to discharge rate modulation decreases as a function of the magnitude and/or the rate of increase in excitatory synaptic input to human motoneurons. Concomitantly, our data suggests that the modulation in the pattern of inhibition facilitates increases in force production, becoming either more reciprocal or less proportional relative to excitatory synaptic inputs. Furthermore, our exploratory analyses using tracked MUs across several contraction levels indicate that the relationship between peak MU discharge rate and their recruitment thresholds is dependent on contraction force and/or the recruitment threshold of a given MU. This suggests that the onion skin phenomenon commonly observed in human MU discharge patterns might not universally apply, at least in the tibialis anterior muscle, which yielded the greatest number of MUs tracked across contraction levels.

Methodological considerations

Though a large number of MUs were identified from decomposition or high density surface EMG, differences in MU yield were demonstrated across contraction levels and muscles as indicated previously (Del Vecchio *et al.*, 2020). Furthermore, the effect of sex on the number of identified MUs appeared evident (Taylor *et al.*, 2022; Lulic-Kuryllo & Inglis, 2022; Jenz *et al.*, 2023), and resulted in a decreased sample size, particularly for the VM (2 female participants with no identified units). Whilst our decomposition results confirm a common occurrence, consideration needs to be given to the sample of the identified MUs when interpreting the results concerning different motor pools. When attempting to track MUs across contraction intensities, the influence of decomposition biases became evident, with the relative difficulty of identifying lower threshold MUs in the presence of higher threshold units (Francic & Holobar, 2021). To counteract this issue, MUs were tracked either across all contraction levels (30/50/70% MVF) or merely between neighbouring levels (30/50 or 50/70% MVF), with the specific uniqueness of MU tracking accounted for in the statistical model. Despite these challenges, analysis of non-tracked and tracked units yielded similar results and represents the first attempt to understand the contribution of motor commands on MU discharge patterns across a wide range of contraction levels. Specifically, the range of contraction levels employed here is much larger than those previously employed in studies attempting to understand the contribution of PICs to self-sustained discharge at various force outputs (Kim *et al.*, 2020; Afsharipour *et al.*, 2020; Orssatto *et al.*, 2021).

Discharge rate modulation with increased force output

Unsurprisingly, the peak discharge rate of identified MUs increased progressively with greater contraction force. However, the peak discharge rates were greater, and increased to a greater extent in TA, reaching values up to ~30 pps on average during contractions to 70% MVF, compared to ~17-18 pps in VL and VM at the same relative

force levels. This is consistent with prior reports from studies using decomposition of intramuscular (Leong *et al.*, 1999) and surface EMG signals (Škarabot *et al.*, 2023*b*), whereby MU discharge rates of the knee extensors only reach ~20-25 pps during maximal effort isometric contractions. The reason for differences in discharge rate between muscles remains unclear; the vastii motor pools might receive a large degree of tonic inhibitory input that is more constant or proportional in its pattern to excitatory input (see below), or the common input might be more evenly distributed in the vastii muscles due to the presumed smaller relative contribution of individual motor pools of the quadriceps to knee extension compared to the relatively greater contribution to TA motor pool to dorsiflexion. That said, these explanations remain highly speculative at present.

To our knowledge, we are the first to explore the relationship between peak discharge rates and recruitment thresholds of MUs across a range of contraction levels, from relatively low to high, for the *same*, tracked motor units. Using this approach, we showed that the relationship between the peak discharge rate and recruitment threshold of a given unit is modulated across contractions to various force levels, presumably to support the need for a given force production. In TA, during contractions up to 30% MVF, the relationship between peak discharge rate and recruitment threshold was negative, supporting the 'onion skin phenomenon' whereby lower threshold MUs exhibit greater peak discharge rates compared to higher threshold units. During the 50% contraction, the relationship between the same MUs (i.e., only those recruited from 0-30% MVF) was flat and non-significant, suggesting convergence or co-modulation of MU discharge rates irrespective of recruitment threshold. Finally, the relationship between the peak discharge rate and recruitment threshold of those same MUs was positive during the 70% contraction level, indicating that higher threshold TA MUs discharge at higher rates compared to lower threshold units. Although this behaviour was clear in TA, it was not replicated in VL and VM. It should be noted, however, that the sample size of tracked MUs across contraction levels was relatively low in VL and VM, which likely reduced statistical power. Considering the low number of MUs that can typically be decomposed in these muscles, recording arrangements with greater density and area (Caillet *et al.*, 2023) will likely be needed in the future to obtain a representative sample of tracked units across contraction levels and thus determine whether the behaviour observed in TA is specific to that motor pool.

Whilst the onion skin phenomenon has been typically observed in human recordings for lower contraction levels (Erim *et al.*, 1996; Hassan *et al.*, 2021), the reverse has also been observed, most notably in studies that utilised higher levels of force (Moritz *et al.*, 2005; Oya *et al.*, 2009; Inglis & Gabriel, 2021). In our study, we extend these observations by showing that even relatively lower threshold MUs (recruitment thresholds <30% MVF) may exhibit reversal of the onion skin phenomenon when the need for force production is sufficiently high. The latter is consistent with the behaviour observed in motoneurons in animal preparations (Kernell *et al.*, 1983; Botterman *et al.*, 1986) and the purported relationship between mechanical properties and recruitment threshold of relatively higher threshold motor units that require greater discharge rates to achieve a fused force (Grimby *et al.*, 1979). Based on our data, it is therefore conceivable that the effective synaptic input to relatively higher threshold units during lower force levels is insufficient for those units to discharge at their full capacity. In contrast, at higher contraction levels the effective synaptic input leads to

greater peak discharge rates, supporting greater force production and allowing for the attainment of fused force.

Changes in onset-offset hysteresis as a function of contraction force

We observed that onset-offset hysteresis (i.e., ΔF) is greater at higher contraction levels, which suggests that the contribution of PICs to self-sustained motoneuron discharge increases as a function of contraction force. These results are consistent with prior reports in the tibialis anterior and gastrocnemius medialis muscles (Orssatto *et al.*, 2021; Goodlich *et al.*, 2023), but contrast reports of no differences in discharge rate hysteresis with increased contraction levels in tibialis anterior and soleus (Kim *et al.*, 2020; Afsharipour *et al.*, 2020). Though the reason for these conflicting findings is difficult to discern, methodological factors are plausible contributors. One major methodological difference resides in the quantification of onset-offset hysteresis, which is dependent on differences in smoothing functions (Beauchamp *et al.*, 2022*a*), the use of a pairwise or unit-wise approach (Hassan *et al.*, 2020), and the use of a composite reporter unit or individual reporter-test unit pairs (Afsharipour *et al.*, 2020). Furthermore, the tracking of MUs across intensities may contribute to the observed differences between studies. Our results agree with a study that reported estimates of ΔF in *tracked* motor units between 10 and 30% MVF (Orssatto *et al.*, 2021), but disagree with those that did not track MUs across contraction levels (Kim *et al.*, 2020; Afsharipour *et al.*, 2020). Nevertheless, even when considering units of higher recruitment threshold where no MU tracking was employed, we showed a relative increase in ΔF with increased contraction levels (see Supplemental File). Lastly, discrepancies with previous studies might be because the range of contraction forces, and thus the range of MU recruitment thresholds, were small (usually 10-30% MVF; Kim et al., 2020; Afsharipour et al., 2020), making it less likely to detect small differences in ΔF.

The observed increase in onset-offset hysteresis in the present study is unlikely to be from greater discharge rates with larger contraction force, as these increases were preserved when ΔF was normalised. Rather than focusing on peak discharge rate (Orssatto *et al.*, 2021), our normalisation involved expressing ΔF estimates as a proportion of the theoretically maximal sustained discharge rate modulation for each test unit (see Figure 1B). We reason that this normalisation more robustly accounts for floor effects as well as the potential confounding of ΔF with discharge rate modulation or self-sustained discharge duration (Afsharipour *et al.*, 2020). Furthermore, as previously proposed, the use of higher threshold MUs with short ascending activation times as test units could overestimate ΔF (Afsharipour *et al.*, 2020). Due to decomposition bias, these biasing effects could be greater at higher contraction levels, which would partially contaminate the observed increase in hysteresis at greater contraction force. However, this phenomenon would have presumably influenced the non-tracked analysis to a greater extent due to the greater prevalence of relatively higher threshold units with shorter activation times. The consistency of results between the non-tracked and tracked units suggests that this potential bias does not explain our observed results.

The relative increase in onset-offset hysteresis with greater contraction level also appeared unimpeded by intrinsic motoneuron properties such as spike frequency adaptation and spike threshold accommodation. Indeed, the relative increase was

maintained in TA when contractions were either matched for total contraction duration or when matched for the rate of force increase (Experiment 2). Prior work has indicated that longer contractions typically lead to an increase in onset-offset hysteresis, while faster rates of force increase tend to diminish it, with these effects attributed to spike frequency adaptation and spike threshold accommodation, respectively. (Vandenberk & Kalmar, 2014). Our data supports this supposition as ΔF was found to be greater in the 'duration-matched' condition (10 s increase/decrease in force) when compared to the 'rate-matched' condition (6 s increase/decrease in force) for effort levels of 30% MVF. Nevertheless, the relative contribution of spike frequency adaptation and spike threshold accommodation to this observation is difficult to distinguish as both phenomena exhibit similar mechanisms (e.g., sodium channel inactivation; Bradley & Somjen, 1961; Miles *et al.*, 2005*b*). Interestingly, however, the effect was not apparent at 70% MVF, whereby ΔF was similar between conditions (increase/decrease in force of 10 and 14 s for duration- and rate-matched conditions, respectively). The significant interaction between contraction level and condition suggests a greater relative increase in ΔF with contraction level in the rate-matched condition, likely due to a greater effect of spike frequency adaptation.

The inconsistencies in the effects of contraction force on estimates of PICs reported in the literature are unlikely to be a consequence of the differences in discharge rate hysteresis in different motor pools, as discrepant results have been found even when examining the same muscle. The relative contribution of monoaminergic inputs likely varies between motor pools (Hounsgaard *et al.*, 1988; Wilson *et al.*, 2015), which could explain lower ΔF in the vastii muscles compared to TA, an observation that was maintained in normalised ΔF. Alternatively, the differences in discharge rate hysteresis between motor pools might reflect functional tuning of motor pools to environmental demands. Nevertheless, though the changes in discharge rate hysteresis as a function of contraction force were less clear in the vastii muscles compared to TA, an increasing trend was still observed and suggests that self-sustained discharge is dependent on contraction force.

Uncoupling the relative contribution of neuromodulation and patterns of inhibition to motoneuron discharge

The input-output relationship of motoneurons governs the discharge characteristics of MUs and is dependent on the intrinsic electrical properties of motoneurons, as well as the pattern and relative contribution of synaptic excitation, inhibition, and neuromodulation (Johnson *et al.*, 2017*b*). Indeed, the increase in onset-offset hysteresis with greater contraction force suggests an increase in PIC magnitudes with greater contraction level. Considering the dependence of PIC magnitude on monoaminergic release (e.g., 5HT; Lee & Heckman, 1998, 2000), the observed behaviour is consistent with the notion of monoamine-mediated (i.e., 5HT and noradrenaline) gain control mechanism of spinal motoneuron discharge to support greater force production needs (Wei *et al.*, 2014). Further considerations are required, however. First, the monoaminergic release tends to be slow (White *et al.*, 1991; Raymond *et al.*, 2001; Hentall *et al.*, 2006) and thus the comparison with pharmacological studies that substantially alter availability of monoamines in the cell is challenging. Second, discharge rate hysteresis (ΔF) largely assesses a particular property of PICs, that is – prolongation of MU discharge (mediated predominantly by persistent calcium currents, Lee & Heckman, 1998b; Bennett et al., 2001; Li & Bennett,

2003; Harvey et al., 2006; ElBasiouny et al., 2006; Moritz et al., 2007). ΔF is less likely to be sensitive to the remaining hallmarks of PIC action on MU discharge, namely, amplification (Lee & Heckman, 2001; Harvey et al., 2006; Kuo et al., 2006), and rate attenuation (Powers & Heckman, 2017). Finally, neuromodulatory inputs are highly diffuse and thus a local and specific inhibitory system is required to fine-tune PIC activation (Johnson & Heckman, 2014).

Despite the observed increases in ΔF with increased contraction force, this trend was reversed for brace height. Brace height effectively quantifies non-linearity of MU discharge modulation (Figure 1C), and thus the reduction in brace height with increased contraction force suggests that, in the presence of a greater excitatory synaptic input, MU discharge patterns become more linear. At least in simulations, brace height appears to tightly predict changes in neuromodulation and is seemingly uninfluenced by the pattern of inhibitory inputs, unlike ΔF (Chardon *et al.*, 2022; Beauchamp *et al.*, 2023). The deviation in linearity that brace height represents is likely the result of monoaminergic mediated PIC facilitation and thus amplification of motoneuron discharge (Powers & Heckman, 2017), which is due to their rapid activation and inactivation properties allowing generation of inward currents (Lee & Heckman, 2001; Harvey *et al.*, 2006; Kuo *et al.*, 2006). The greater linearity of discharge patterns with greater contraction force indicates a relatively smaller contribution of PICs to motoneuron discharge when requirements for excitatory synaptic input are greater. However, the action of PIC is time-dependent, with sufficient time required for them to be fully activated. This is evident when comparing triangular contractions of different durations, but similar levels of force output; a 10 second increase in force to 30% MVF resulted in less linear discharge rate modulation (greater brace height) compared to a 6 second increase, and similar results were observed when comparing 14 vs. 10 second increase in force up to 70% MVF (Experiment 2, Figure 4H). Nevertheless, the trend of discharge patterns becoming more linear with greater contraction force was maintained even when accounting for the rate of force increase, suggesting that both the magnitude and the rate of increase of excitatory synaptic input influence the relative contribution of neuromodulatory inputs to the linearity of motoneuron discharge.

In addition to neuromodulatory inputs, the extent and pattern of inhibitory relative to excitatory inputs need to be considered when interpreting our data. The large number and density of inhibitory synapses near voltage-sensitive channels responsible for PICs suggest a potent effect of inhibitory inputs on PIC-mediated gain control (Johnson & Heckman, 2014). The inhibitory inputs are thought to either covary with (proportional inhibition; (Berg *et al.*, 2007), or reduce in contrast to (reciprocal inhibition; Johnson et al., 2012) excitatory synaptic input. The rate attenuation slopes, reflective of inhibitory patterns (Beauchamp *et al.*, 2022*b*; Chardon *et al.*, 2022), were largely shown to be reduced as a function of contraction force, suggesting the pattern of inhibition is modulated to support greater force production, by becoming either less proportional or more reciprocal in nature. In either case, this suggests reduced inhibitory synaptic inputs with respect to excitatory inputs at higher forces. Though the source of these inhibitory inputs is elusive and requires further investigation, reciprocal Ia inhibition (Hyngstrom *et al.*, 2007) and recurrent (Renshaw cell) inhibition (Johnson & Heckman, 2014) are thought to be potent mediators of PIC contribution to motoneuron discharge. The pattern of inhibition becoming less proportional or more reciprocal might also be a contributor to the greater calcium PIC persistence and thus

prolongation of MU discharge (Chardon *et al.*, 2022), resulting in greater onset-offset hysteresis with greater contraction forces observed in this study.

Conclusions

Modifications in motor unit behaviour with greater contraction force appears to be mediated by intrinsic properties of the motoneuron as well as alterations in motor commands (i.e., the pattern of excitatory and/or inhibitory synaptic inputs). As contraction force is increased, we found an increase in self-sustained discharge, likely facilitated by calcium PICs, and more linear MU discharge patterns. A multi-metric analysis approach suggests that these changes in linearity could be mediated by smaller relative contributions of PICs and/or more reciprocal or less proportional pattern of inhibition relative to excitatory inputs. This interpretation is supported by relying on *multiple* metrics to estimate the relative contribution of different components of motor commands to MU discharge behaviour and suggests that modulation of contraction force is orchestrated by a uniquely shaped combination of excitatory and inhibitory synaptic input, as well as neuromodulation.

REFERENCES

Afsharipour B, Manzur N, Duchcherer J, Fenrich KK, Thompson CK, Negro F, Quinlan KA, Bennett DJ & Gorassini MA (2020). Estimation of self-sustained activity produced by persistent inward currents using firing rate profiles of multiple motor units in humans. *J Neurophysiol* **124,** 63–85.

Bakdash JZ & Marusich LR (2017). Repeated Measures Correlation. *Front Psychol*; DOI: 10.3389/FPSYG.2017.00456.

Bates D, Mächler M, Bolker BM & Walker SC (2015). Fitting Linear Mixed-Effects Models using lme4. *J Stat Softw*; DOI: 10.48550/arxiv.1406.5823.

Beauchamp JA, Khurram OU, Dewald JPA, Heckman CJ & Pearcey GEP (2022*a*). A computational approach for generating continuous estimates of motor unit discharge rates and visualizing population discharge characteristics. *J Neural Eng*; DOI: 10.1088/1741-2552/AC4594.

Beauchamp JA, Pearcey GEP, Khurram OU, Chardon M, Wang YC, Powers RK, Dewald JPA & Heckman CJ (2023). A geometric approach to quantifying the neuromodulatory effects of persistent inward currents on individual motor unit discharge patterns. *J Neural Eng*; DOI: 10.1088/1741-2552/ACB1D7.

Beauchamp JamesA, Pearcey GEP, Khurram OU, Chardon M, Wang C, Powers RK, Dewald JPA & Heckman CJ (2022*b*). A geometric approach to quantifying the neuromodulatory effects of persistent inward currents on single motor unit discharge patterns. *bioRxiv*doi.org/10.1101/2022.10.06.511149.

Bennett DJ, Hultborn H, Fedirchuk B & Gorassini M (1998). Synaptic activation of plateaus in hindlimb motoneurons of decerebrate cats. *J Neurophysiol* **80,** 2023–2037.

Bennett DJ, Li Y, Harvey PJ & Gorassini M (2001). Evidence for Plateau Potentials in Tail Motoneurons of Awake Chronic Spinal Rats With Spasticity. *J Neurophysiol* **86,** 1972–1982.

Berg RW, Alaburda A & Hounsgaard J (2007). Balanced inhibition and excitation drive spike activity in spinal half-centers. *Science* **315,** 390–393.

Binder MD, Powers RK & Heckman CJ (2020). Nonlinear Input-Output Functions of Motoneurons. *Physiology (Bethesda)* **35,** 31–39.

Botterman BR, Iwamoto GA & Gonyea WJ (1986). Gradation of isometric tension by different activation rates in motor units of cat flexor carpi radialis muscle. *J Neurophysiol* **56,** 494–506.

Bradley K & Somjen GG (1961). Accommodation in motoneurones of the rat and the cat. *J Physiol* **156,** 75–92.

Caillet AH, Avrillon S, Kundu A, Yu T, Phillips ATM, Modenese L & Farina D (2023). Larger and Denser: An Optimal Design for Surface Grids of EMG Electrodes to Identify Greater and More Representative Samples of Motor Units. *eNeuro* **10,** ENEURO.0064-23.2023.

Chardon MK, Wang YC, Garcia M, Besler E, Beauchamp JA, D'Mello M, Powers RK & Heckman CJ (2022). Supercomputers and Reverse Engineering of Motoneuron Firing Patterns. *bioRxiv*2022.12.09.519818.

Cheney PD & Fetz EE (1980). Functional classes of primate corticomotoneuronal cells and their relation to active force. *J Neurophysiol* **44,** 773–791.

ElBasiouny SM, Bennett DJ & Mushahwar VK (2006). Simulation of Ca2+ persistent inward currents in spinal motoneurones: mode of activation and integration of synaptic inputs. *J Physiol* **570,** 355–374.

Erim Z, De Luca CJ, Mineo K & Aoki T (1996). Rank-ordered regulation of motor units. *Muscle Nerve* **19,** 563–573.

Farina D, Holobar A, Merletti R & Enoka RM (2010). Decoding the neural drive to muscles from the surface electromyogram. *Clinical Neurophysiology* **121,** 1616–1623.

Francic A & Holobar A (2021). On the reuse of motor unit filters in high density surface electromyograms recorded at different contraction levels. *IEEE Access* **9,** 115227–115236.

Glover IS & Baker SN (2022). Both Corticospinal and Reticulospinal Tracts Control Force of Contraction. *J Neurosci*JN-RM-0627-21.

Goaillard JM & Marder E (2021). Ion Channel Degeneracy, Variability, and Covariation in Neuron and Circuit Resilience. *Annu Rev Neurosci* **44,** 335–357.

Goodlich BI, Del Vecchio A, Horan SA & Kavanagh JJ (2023). Blockade of 5-HT2 receptors suppresses motor unit firing and estimates of persistent inward currents during voluntary muscle contraction in humans. *J Physiol*; DOI: 10.1113/JP284164.

Gorassini M, Yang JF, Siu M & Bennett DJ (2002*a*). Intrinsic activation of human motoneurons: possible contribution to motor unit excitation. *J Neurophysiol* **87,** 1850–1858.

Gorassini M, Yang JF, Siu M & Bennett DJ (2002*b*). Intrinsic activation of human motoneurons: Reduction of motor unit recruitment thresholds by repeated contractions. *J Neurophysiol* **87,** 1859–1866.

Gorassini MA, Bennett DJ & Yang JF (1998). Self-sustained firing of human motor units. *Neurosci Lett* **247,** 13–16.

Gorassini MA, Knash ME, Harvey PJ, Bennett DJ & Yang JF (2004). Role of motoneurons in the generation of muscle spasms after spinal cord injury. *Brain* **127,** 2247–2258.

Grimby L & Hannerz J (1977). Firing rate and recruitment order of toe extensor motor units in different modes of voluntary conraction. *J Physiol* **264,** 865–879.

Grimby L, Hannerz J & Hedman B (1979). Contraction time and voluntary discharge properties of individual short toe extensor motor units in man. *J Physiol* **289,** 191–201.

Harvey PJ, Li Y, Li X & Bennett DJ (2006). Persistent sodium currents and repetitive firing in motoneurons of the sacrocaudal spinal cord of adult rats. *J Neurophysiol* **96,** 1141–1157.

Hassan A, Thompson CK, Negro F, Cummings M, Powers RK, Heckman CJ, Dewald JPA & McPherson LM (2020). Impact of parameter selection on estimates of motoneuron excitability using paired motor unit analysis. *J Neural Eng*; DOI: 10.1088/1741-2552/AB5EDA.

Hassan AS, Fajardo ME, Cummings M, McPherson LM, Negro F, Dewald JPA, Heckman CJ & Pearcey GEP (2021). Estimates of persistent inward currents are reduced in upper limb motor units of older adults. *J Physiol* **599,** 4865–4882.

Heckman CJ & Enoka RM (2012). Motor unit. *Compr Physiol* **2,** 2629–2682.

Hentall ID, Pinzon A & Noga BR (2006). Spatial and temporal patterns of serotonin release in the rat's lumbar spinal cord following electrical stimulation of the nucleus raphe magnus. *Neuroscience* **142,** 893–903.

Holobar A, Minetto M, Botter A, Negro F & Farina D (2010). Experimental analysis of accuracy in the identification of motor unit spike trains from high-density surface EMG. *IEEE Trans Neural Syst Rehabil Eng* **18,** 221–229.

Holobar A, Minetto MA & Farina D (2014). Accurate identification of motor unit discharge patterns from high-density surface EMG and validation with a novel signal-based performance metric. *J Neural Eng* **11,** 016008.

Holobar A & Zazula D (2007). Multichannel blind source separation using convolution Kernel compensation. *IEEE Transactions on Signal Processing* **55,** 4487–4496.

Hounsgaard J, Hultborn H, Jespersen B & Kiehn O (1988). Bistability of alpha-motoneurones in the decerebrate cat and in the acute spinal cat after intravenous 5-hydroxytryptophan. *J Physiol* **405,** 345–367.

Hultborn H, Brownstone RB, Toth TI & Gossard JP (2004). Key mechanisms for setting the input-output gain across the motoneuron pool. *Prog Brain Res* **143,** 75–95.

Hyngstrom AS, Johnson MD, Miller JF & Heckman CJ (2007). Intrinsic electrical properties of spinal motoneurons vary with joint angle. *Nat Neurosci* **10,** 363–369.

Inglis JG & Gabriel DA (2021). Is the "reverse onion skin" phenomenon more prevalent than we thought during intramuscular myoelectric recordings from low to maximal force outputs? *Neurosci Lett*; DOI: 10.1016/J.NEULET.2020.135583.

Jacobs BL, Martín-Cora FJ & Fornal CA (2002). Activity of medullary serotonergic neurons in freely moving animals. *Brain Res Rev* **40,** 45–52.

Jenz ST, Beauchamp JA, Gomes MM, Negro F, Heckman CJ & Pearcey GEP (2023). Estimates of persistent inward currents in lower limb motoneurons are larger in females than in males. *J Neurophysiol* **129,** 1322–1333.

Johnson MD & Heckman CJ (2014). Gain control mechanisms in spinal motoneurons. *Front Neural Circuits*; DOI: 10.3389/fncir.2014.00081.

Johnson MD, Hyngstrom AS, Manuel M & Heckman CJ (2012). Push-pull control of motor output. *J Neurosci* **32,** 4592–4599.

Johnson MD, Thompson CK, Tysseling VM, Powers RK & Heckman CJ (2017*a*). The potential for understanding the synaptic organization of human motor commands via the firing patterns of motoneurons. *J Neurophysiol* **118,** 520–531.

Johnson MD, Thompson CK, Tysseling VM, Powers RK & Heckman CJ (2017*b*). The potential for understanding the synaptic organization of human motor commands via the firing patterns of motoneurons. *J Neurophysiol* **118,** 520–531.

Kavanagh JJ, McFarland AJ & Taylor JL (2019). Enhanced availability of serotonin increases activation of unfatigued muscle but exacerbates central fatigue during prolonged sustained contractions. *J Physiol* **597,** 319–332.

Kernell D, Eerbeek O & Verhey BA (1983). Relation between isometric force and stimulus rate in cat's hindlimb motor units of different twitch contraction time. *Exp Brain Res* **50,** 220–227.

Khurram OU, Pearcey GEP, Chardon MK, Kim EH, García M & Heckman CJ (2022). The Cellular Basis for the Generation of Firing Patterns in Human Motor Units. *Adv Neurobiol* **28,** 233–258.

Kim EH, Wilson JM, Thompson CK & Heckman CJ (2020). Differences in estimated persistent inward currents between ankle flexors and extensors in humans. *J Neurophysiol* **124,** 525–535.

Kuo JJ, Lee RH, Johnson MD, Heckman HM & Heckman CJ (2003). Active dendritic integration of inhibitory synaptic inputs in vivo. *J Neurophysiol* **90,** 3617–3624.

Kuo JJ, Lee RH, Zhang L & Heckman CJ (2006). Essential role of the persistent sodium current in spike initiation during slowly rising inputs in mouse spinal neurones. *J Physiol* **574,** 819–834.

Kuznetsova A, Brockhoff PB & Christensen RHB (2017). lmerTest Package: Tests in Linear Mixed Effects Models. *J Stat Softw* **82,** 1–26.

Lee RH & Heckman CJ (1998*a*). Bistability in spinal motoneurons in vivo: Systematic variations in persistent inward currents. *J Neurophysiol* **80,** 583–593.

Lee RH & Heckman CJ (1998*b*). Bistability in spinal motoneurons in vivo: systematic variations in persistent inward currents. *J Neurophysiol* **80,** 583–593.

Lee RH & Heckman CJ (2000). Adjustable amplification of synaptic input in the dendrites of spinal motoneurons in vivo. *J Neurosci* **20,** 6734–6740.

Lee RH & Heckman CJ (2001). Essential role of a fast persistent inward current in action potential initiation and control of rhythmic firing. *J Neurophysiol* **85,** 472–475.

Lenth R & Lenth M (2018). Package 'lsmeans.' *American Statistician* **34,** 216–221.

Leong B, Kamen G, Patten C & Burke JR (1999). Maximal motor unit discharge rates in the quadriceps muscles of older weight lifters. *Med Sci Sports Exerc* **31,** 1638–1644.

Li X & Bennett DJ (2007). Apamin-sensitive calcium-activated potassium currents (SK) are activated by persistent calcium currents in rat motoneurons. *J Neurophysiol* **97,** 3314–3330.

Li Y & Bennett DJ (2003). Persistent sodium and calcium currents cause plateau potentials in motoneurons of chronic spinal rats. *J Neurophysiol* **90,** 857–869.

Li Y, Gorassini MA & Bennett DJ (2004). Role of persistent sodium and calcium currents in motoneuron firing and spasticity in chronic spinal rats. *J Neurophysiol* **91,** 767–783.

Lulic-Kuryllo T & Inglis JG (2022). Sex differences in motor unit behaviour: A review. *J Electromyogr Kinesiol*; DOI: 10.1016/J.JELEKIN.2022.102689.

Mesquita RNO, Taylor JL, Trajano GS, Škarabot J, Holobar A, Gonçalves BAM & Blazevich AJ (2022). Effects of reciprocal inhibition and whole-body relaxation on persistent inward currents estimated by two different methods. *J Physiol* **600,** 2765–2787.

Miles GB, Dai Y & Brownstone RM (2005*a*). Mechanisms underlying the early phase of spike frequency adaptation in mouse spinal motoneurones. *J Physiol* **566,** 519–532.

Miles GB, Dai Y & Brownstone RM (2005*b*). Mechanisms underlying the early phase of spike frequency adaptation in mouse spinal motoneurones. *J Physiol* **566,** 519–532.

Moritz AT, Newkirk G, Powers RK & Binder MD (2007). Facilitation of somatic calcium channels can evoke prolonged tail currents in rat hypoglossal motoneurons. *J Neurophysiol* **98,** 1042–1047.

Moritz CT, Barry BK, Pascoe MA & Enoka RM (2005). Discharge rate variability influences the variation in force fluctuations across the working range of a hand muscle. *J Neurophysiol* **93,** 2449–2459.

Orssatto LBR, Mackay K, Shield AJ, Sakugawa RL, Blazevich AJ & Trajano GS (2021). Estimates of persistent inward currents increase with the level of voluntary drive in low-threshold motor units of plantar flexor muscles. *J Neurophysiol* **125,** 1746–1754.

Oya T, Hoffman B & Cresswell A (2008). Corticospinal-evoked responses in lower limb muscles during voluntary contractions at varying strengths. *Journal of Applied Physiology (1985)* **115,** 1527–1532.

Oya T, Riek S & Cresswell AG (2009). Recruitment and rate coding organisation for soleus motor units across entire range of voluntary isometric plantar flexions. *J Physiol* **587,** 4737–4748.

Pearcey GE & Rymer WZ (2022). Population recordings of human motor units often display “onion skin” discharge patterns -- implications for voluntary motor control. *ArXiv*. Available at: https://arxiv.org/abs/2208.11783v1 [Accessed June 8, 2023].

Pearcey GEP, Khurram OU, Beauchamp JA, Negro F & Heckman CJ (2022). Antagonist tendon vibration dampens estimates of persistent inward currents in motor units of the human lower limb. *bioRxiv*2022.08.02.502526.

Person RS & Kudina LP (1972). Discharge frequency and discharge pattern of human motor units during voluntary contraction of muscle. *Electroencephalogr Clin Neurophysiol* **32,** 471–483.

Powers RK, Elbasiouny SM, Zev Rymer W & Heckman CJ (2012). Contribution of intrinsic properties and synaptic inputs to motoneuron discharge patterns: a simulation study. *J Neurophysiol* **107,** 808–823.

Powers RK & Heckman CJ (2017). Synaptic control of the shape of the motoneuron pool input-output function. *J Neurophysiol* **117,** 1171–1184.

Powers RK, Sawczuk A, Musick JR & Binder MD (1999). Multiple mechanisms of spike-frequency adaptation in motoneurones. *J Physiol Paris* **93,** 101–114.

Raymond JR, Mukhin Y V., Gelasco A, Turner J, Collinsworth G, Gettys TW, Grewal JS & Garnovskaya MN (2001). Multiplicity of mechanisms of serotonin receptor signal transduction. *Pharmacol Ther* **92,** 179–212.

Revill AL & Fuglevand AJ (2011). Effects of persistent inward currents, accommodation, and adaptation on motor unit behavior: a simulation study. *J Neurophysiol* **106,** 1467–1479.

Revill AL & Fuglevand AJ (2017). Inhibition linearizes firing rate responses in human motor units: implications for the role of persistent inward currents. *Journal of Physiology* **595,** 179–191.

Sawczuk A, Powers R & Binder M (1995). Spike frequency adaptation studied in hypoglossal motoneurons of the rat. *J Neurophysiol* **73,** 1799–1810.

Schwindt PC & Crill WE (1980). Properties of a persistent inward current in normal and TEA-injected motoneurons. *J Neurophysiol* **43,** 1700–1724.

Sherrington CS (1925). Remarks on some Aspects of Reflex Inhibition. *Proceedings of the Royal Society of London Series B, Containing Papers of a Biological*

Character **97,** 519–545. Available at: https://www.jstor.org/stable/pdf/81057.pdf [Accessed February 25, 2020].

Škarabot J, Ammann C, Balshaw TG, Divjak M, Urh F, Murks N, Foffani G & Holobar A (2023*a*). Decoding firings of a large population of human motor units from high-density surface electromyogram in response to transcranial magnetic stimulation. *J Physiol*; DOI: 10.1113/JP284043.

Škarabot J, Folland JP, Forsyth J, Vazoukis A, Holobar A & Del Vecchio A (2023*b*). Motor unit discharge characteristics and conduction velocity of the vastii muscles in long-term resistance-trained men. *Med Sci Sports Exerc*; DOI: 10.1249/MSS.0000000000003105.

Stephenson JL & Maluf KS (2011). Dependence of the paired motor unit analysis on motor unit discharge characteristics in the human tibialis anterior muscle. *J Neurosci Methods* **198,** 84–92.

Taylor CA, Kopicko BH, Negro F & Thompson CK (2022). Sex differences in the detection of motor unit action potentials identified using high-density surface electromyography. *J Electromyogr Kinesiol*; DOI: 10.1016/J.JELEKIN.2022.102675.

Vandenberk MS & Kalmar JM (2014). An evaluation of paired motor unit estimates of persistent inward current in human motoneurons. *J Neurophysiol* **111,** 1877–1884.

Del Vecchio A, Holobar A, Falla D, Felici F, Enoka RM & Farina D (2020). Tutorial: Analysis of motor unit discharge characteristics from high-density surface EMG signals. *Journal of Electromyography and Kinesiology* **53,** 102426.

Weavil J, Sidhu S, Mangum T, Richardson R & Amann M (2015). Intensity-dependent alterations in the excitability of cortical and spinal projections to the knee extensors during isometric and locomotor exercise. *Am J Physiol Regul Integr Comp Physiol* **308,** 998–1007.

Wei K, Glaser JI, Deng L, Thompson CK, Stevenson IH, Wang Q, Hornby TG, Heckman CJ & Kording KP (2014). Serotonin affects movement gain control in the spinal cord. *J Neurosci* **34,** 12690–12700.

White SR, Fung SJ & Barnes CD (1991). Norepinephrine effects on spinal motoneurons. *Prog Brain Res* **88,** 343–350.

Wilson JM, Thompson CK, Miller LC & Heckman CJ (2015). Intrinsic excitability of human motoneurons in biceps brachii versus triceps brachii. *J Neurophysiol* **113,** 3692–3699.

Author contributions

J.Š. and G.E.P.P. conceived and designed the work; J.Š. performed experiments; all authors analysed data; all authors interpreted results; J.Š. drafted the manuscript; all authors revised the manuscript.

Grants

J.Š. is supported by Versus Arthritis Foundation Fellowship (reference: 22569). G.E.P.P. is supported by the Natural Sciences and Engineering Research Council of Canada (Discovery Grant RGPIN-2023-05862, and Discovery Launch Supplement DGECR-2023-00279).

Acknowledgments

The authors are grateful to Miss Tamara Valenčič, Mr Chris Connelly, and Mr Haydn Thomason for assistance with data collection.

Conflict of interest

The authors declare no conflict of interest, financial or otherwise.